Modeling Spontaneous Metastasis following Surgery: An In Vivo-In Silico Approach

Sébastien Benzekry, Amanda Tracz, Michalis Mastri, R. Corbelli, Dominique Barbolosi, John Ebos

Modeling spontaneous metastasis following surgery: an *in vivo-in silico* approach

Sebastien Benzekry[1], Amanda Tracz[2], Michalis Mastri[2], Ryan Corbelli[2], Dominique Barbolosi[4], and John ML Ebos[2,3]

[1]inria Bordeaux Sud-Ouest, team MONC, Institut de Mathematiques de Bordeaux, Bordeaux, France

[2]Department of Cancer Genetics, [3]Department of Medicine, Roswell Park Cancer Institute, Elm & Carlton Streets, Buffalo, NY, USA

[4]SMARTc Pharmacokinetics Unit, Inserm S 911 CRO2, Aix Marseille University, Marseille, France

Running title: Modeling the impact of surgery on metastasis

Wordcounts:

Abstract: 240/350 words

Quick guide to equations and assumptions: 731/800 words

Body text: 4995/5000 words

Abstract

Rapid improvements in the detection and tracking of early-stage tumor progression aim to guide decisions regarding cancer treatments as well as predict metastatic recurrence in patients following surgery. Mathematical models may have the potential to further assist in estimating metastatic risk, particularly when paired with in vivo tumor data that faithfully represent all stages of disease progression. Herein we describe mathematical analysis that uses data from mouse models of spontaneous metastasis developing after surgical removal of orthotopically implanted primary tumors. Both presurgical (primary tumor) and postsurgical (metastatic) growth was quantified using bioluminescence and was then used to generate a mathematical formalism based on general laws of the disease (i.e. dissemination and growth). The model was able to fit and predict pre-/post-surgical data at the level of the individual as well as the population. Our approach also enabled retrospective analysis of clinical data describing the probability of metastatic relapse as a function of primary tumor size. In these data-based models, inter-individual variability was quantified by a key parameter of intrinsic metastatic potential. Critically, our analysis identified a highly nonlinear relationship between primary tumor size and postsurgical survival, suggesting possible threshold limits for the utility of tumor size as a predictor of metastatic recurrence. These findings represent a novel use of clinically relevant models to assess the impact of surgery on metastatic potential and may guide optimal timing of treatments in neoadjuvant (presurgical) and adjuvant (postsurgical) settings to maximize patient benefit.

Précis: A data-based mathematical model that assesses the impact of surgery on metastatic development may have clinical uses to individualize adjuvant therapies that can extend cancer remission.

Introduction

Surgical removal of an early-stage localized tumor remains one of the most effective strategies in reducing the probability of systemic metastatic disease spread (1). Improved technologies of early cancer detection aim to classify primary tumor stage to identify whether potential treatment modalities – such as presurgical 'neoadjvuant' or postsurgical 'adjuvant' – should be considered to complement surgery and reduce metastatic potential. However the relationship between primary tumor growth and eventual metastasis remains enigmatic (2). Metastatic seeding was initially thought to occur only during late stages of primary tumor growth and invasion (3), however, recent evidence suggests systemic dissemination is a much earlier event (4). Indeed even the direction of tumor spread, initially thought to occur uni-directionally from primary to secondary sites, has been replaced by more complex and dynamic theories of interaction. These include models where primary and secondary lesions grow (and evolve) in parallel (2) and the possibility that cell seeding can be bi-directional, with metastasis potentially 're-seeding' back to original primary location (5,6).

To assist in understanding this complexity, mathematical modeling has been used to determine the relationship between primary (localized) and secondary (metastatic) tumor dissemination and growth. Early studies used statistical analyses only (7,8), while later work included experimentally-derived data to validate models using biological information that aimed to more faithfully represent the metastatic process (9). In 2000, Iwata and colleagues used imaging data from one patient with metastatic hepatocellular carcinoma to introduce a more formalistic and biologically-based approach that relied on the description of the temporal dynamics of a population of metastatic colonies, with equations written at the organ or organism scale (10). In

parallel, several studies have sought to include additional variables when modeling tumor growth, such as angiogenesis (11), stem cell behavior (12), tumor-immune interactions (13) and microenvironment influences (14), among numerous others. To date, the majority of mathematical studies in cancer modeling have focused on primary tumor and relatively few have investigated the metastatic development (15-22).

This dearth in metastatic data stems largely from the complexity of studying metastasis itself. Metastasis starts with localized primary tumor growth which then invades and intravasates into the bloodstream which, in turn, spreads systemically until extravating into tissue at a distant (hospitable) site (23,24). While clinical (retrospective) data has value (2,7,20,25,26), mouse tumor models have typically aimed to mimic (and distinguish between) several stages of the metastatic process. In certain mouse models, metastasis can derive from a tumor that is implanted ectopically or orthotopically into a primary or metastatic site ('ectopic', 'orthotopic' or 'ortho-metastatic' models, respectively (27)) and can involve various immune states (i.e., human xenograft or mouse isograft). Although more rarely performed, models can also include surgical resection of the primary tumor which allows for progression of clinically relevant spontaneous metastatic disease. These can include surgery following ectopic implantation (i.e., 'ecto-surgical', such as tumors grown in the ear or limb that are later amputated), or orthotopic implantation and resection (i.e., 'ortho-surgical'), which more faithfully represent patient disease. To date, no studies have utilized data from ortho-surgical metastasis models for mathematical analysis.

Herein we describe a mathematical approach developed using data derived from two ortho-surgical metastasis models representing competent and incompetent immune systems with luciferase-tagged human breast (LM2-4^{LUC+}) and mouse kidney (RENCA^{LUC+}) cell lines. We first defined a mathematical formalism from basic laws of

the disease (dissemination and growth). Then we confronted the mathematical outputs to longitudinal measurements of primary tumor size, metastatic burden and survival using a population approach (nonlinear mixed-effects) for statistical estimation of the parameters. Minimally parameterized models of each experimental system were generated and used to fit and predict pre-/post-surgical data at the individual and population levels. Next we used clinical datasets to assess metastatic relapse probability from primary tumor size and show that, in both cases (preclinical and clinical), one specific parameter (μ) allowed quantification of inter-animal/individual variability in metastatic propensity. Critically, our models confirm a strong dependence between presurgical primary tumor size and postsurgical metastatic growth and survival. However, quantitative analysis revealed a highly nonlinear pattern in this dependency and identified a range of tumor sizes (either large or small) where variation of tumor size did not significantly impact on survival. These represent potential threshold limits for the utility of primary size as a predictor of metastatic disease (i.e., if small, then surgical cure; if large, then surgical redundancy). These findings represent the first time clinically relevant surgical models have been integrated with data-based mathematical models to inform the quantitative impact of presurgical primary tumor size on subsequent metastatic disease.

Quick guide to equations and assumptions

The metastatic modeling approach we employed follows the formalism initiated by Iwata et al. (10), which was further developed/expanded in recent works in two key ways: 1) effect of systemic therapies (28,29), and 2) use in a (non-surgical) *in vivo* human xenograft model involving orthotopic primary tumors (PTs) and metastasis (21). Metastatic development is reduced to two main components:

1) Growth: includes presurgical primary (g_p) and secondary (g) tumor growth rates

2) Dissemination: includes metastatic dissemination rate (d).

A schematic description of the model is depicted in Figure 1. More complex considerations on the biology (1,30) and modeling (31) of the metastatic process have been considered elsewhere.

Growth dynamics

The PT volume $V_p(t)$ solves the following equations

$$\begin{cases} \frac{dV_p}{dt} = g_p(V_p) \\ V_p(t=0) = V_i \end{cases} \quad (1)$$

The initial condition for the PT, denoted by V_i, was determined either by the number of injected cells (preclinical case) or the initial tumor size at inception (clinical case, $V_i = 1$ cell). Metastases were assumed to start from one cell. For each case, the optimal structure resulting from our investigations was to assume the same structural law for the PT and the metastases, although with possibly different parameter values.

Preclinical : Human breast (LM2-4^{LUC+}) metastasis model

Growth dynamics were defined by

1) Gomp-Exp (32) growth model (see expression below)

2) Growth parameters for PT and metastases treated identically ($g = g_p$)

In a previous study quantifying the descriptive power of several growth kinetics models using data from the same breast animal model (33), the Gompertz model accurately described primary tumor growth curves, in accordance with a large body of literature (see references in (33)). However, a limitation of this model is that the tumor doubling time could become arbitrarily small for small volumes, a feature that we considered biologically irrelevant for small volumes at metastatic initiation (of the order of the cell). A lower bound to this doubling time might be expressed by the *in vitro* doubling time of the cell line, which can be experimentally determined. Consequently, we adopted the Gomp-Exp model (32), defined by

$$g_p(v) = g(v) = \min\left(\lambda v, \left(\alpha - \beta \ln\left(\frac{v}{V_0}\right)\right) v\right) \quad (2)$$

Under this model, growth is divided between two phases: an initial exponential phase, followed by a Gompertz growth phase. Parameter λ is the maximal proliferation rate, taken here to be equal to the value inferred from *in vitro* proliferation assays (see supplementary Figure 1A and Table 2). The second term in the min function is the Gompertz growth rate, defined by two parameters. Parameter α is the intrinsic relative (specific) growth rate at the size V_0 of one cell. Parameter β is the exponential decay rate of the relative (specific) growth rate.

Preclinical : Mouse kidney (RENCA^{LUC+}) metastasis model

Growth dynamics were defined by

1) Exponential growth model.

2) Growth parameters for PT and metastases treated differently.

In mathematical terms, this is expressed by

$$g_p(v) = \alpha_p v, \qquad g(v) = \alpha v \tag{3}$$

Clinical : Human metastatic breast data

Growth dynamics were defined by

1) Gompertz growth model

2) Growth parameters for PT and metastases treated identically ($g_p = g$)

Metastatic dissemination

The formation of new metastases was assumed to occur at a PT volume-dependent rate $d(V_p)$ having the following parametric expression

$$d(V_p) = \mu V_p \tag{4}$$

where parameter μ is an intrinsic parameter of metastatic aggressiveness. This critical coefficient is the daily probability for a given tumor cell to successfully establish a metastasis. Therefore it is the product of several probabilities: 1) the probability of having evolved the necessary genetic mutations to ensure the phenotypic abilities required at each step of the metastatic process, 2) the survival probability of all adverse events occurring in transit including survival in the blood or immune escape, among others, and 3) the probability to generate a functional colony at the distant site. Following reported observations (34), we assumed that all the metastases were growing at the same volume (v)-dependent rate $g(v)$ and that they all started from the same volume corresponding to the volume of one cell. The population of metastases was then formalized by means of a time (t)-dependent volume distribution $\rho(t, v)$ solving the following problem (10):

$$\begin{cases} \partial_t \rho(t,v) + \partial_v\big(\rho(t,v)g(v)\big) = 0 & t \in (0,+\infty),\ \ v \in (V_0,+\infty) \\ g(V_0)\rho(t,V_0) = d\left(V_p(t)\right) & t \in (0,+\infty) \\ \rho(0,v) = 0 & v \in (V_0,+\infty) \end{cases}$$

$$N(t) = \int_{V_0}^{+\infty} \rho(t,v)dv = \int_0^t d\left(V_p(s)\right)ds = \mu \int_0^t V_p(s)ds\,, \tag{5}$$

$$M(t) = \int_{V_0}^{+\infty} v\rho(t,v)dv = \int_0^t d\left(V_p(t-s)\right)V(s)ds$$

The first equation is a continuity equation expressing conservation of the number of metastases when they grow. The second equation is a Neumann boundary condition on the flux of entering metastases at size $V = V_0$. The third equation describes the initial condition (no metastases at the initial time). From the solution of this problem two main macroscopic quantities can be derived, the metastatic burden $M(t)$ and the number of metastases $N(t)$. In the convolution formula for $M(t)$ (35), $V(s)$ represents a solution to the Cauchy problem (1) with g instead of g_p and V_0 as initial condition. This formula allows fast simulation of the model using the fast Fourier transform algorithm (35), which was essential for estimation of the parameters that required a very large number of model evaluations.

Materials and methods

Preclinical Methodology

Cell lines

The human LM2-4^{LUC+} cells are a luciferase-expressing metastatic variant of the MDA-MB-231 breast cancer-cell line derived after multiple rounds of *in vivo* lung metastasis selection in mice, as previously described (see (36) (37)). Mouse kidney RENCA^{LUC+} cells expressing luciferase were a kind gift from R.Pili, Roswell Park Cancer Institute and described previously (38). LM2-4^{LUC+} and RENCA^{LUC+} were maintained in Dulbecco's modified Eagle's medium (Corning, Cat. #MT10-013-CV) and in RPMI (Roswell Park Memorial Institute) medium (Corning, Cat. #MT15-041-CV), respectively, with 5% heat-inactivated fetal bovine serum (Corning, Cat. #MT35-010-CV). Cells were authenticated by STR profile comparison to ATCC parental cell database (for LM2-4^{LUC+}) or confirmation of species origin (for RENCA^{LUC+}) (DDC Medical, USA). All cells were incubated at 37°C and 5% CO2 in a humidified incubator.

Cell Proliferation assay

LM2-4^{LUC+} cells were plated in 35mm plates (5x10^5 cells per plate) and were manually counted using trypan blue staining every 24 hours for 72 hours total (cellgro, Cat. #25-900-CI).

Photon-to-cell ratio

LM2-4^{LUC+} cells were trypsinized and counted. 5x10^6 cells were serial diluted 2 fold down to 9.77x10^3 cells and processed with Bright-Glo Luciferase Assay System (Promega, Cat. #E2610) following manufacture's protocol.

Ortho-surgical models of metastasis

Animal tumor model studies were performed in strict accordance with the recommendations in the Guide for Care and Use of Laboratory Animals of the National Institutes of Health and according to guidelines of the institutional Animal Care and Use Committee (IACUC) at Roswell Park Cancer Institute (Protocol: 1227M, to JMLE).

The optimization and use of animal models of breast and kidney metastasis orthotopic primary tumor implantation and surgical resection have been extensively detailed elsewhere (39). Briefly, LM2-4^{LUC+} cells (2x10^6 cells in 50µL) and RENCA^{LUC+} (4x10^4 cells in 5µL) were implanted, respectively, into the right inguinal mammary fat pad (right flank) or kidney (subcapsular space) of 6-8 week old female CB-17 SCID or Balb/c mice(39). Primary breast tumor size was assessed regularly with Vernier calipers using the formula width^2(length×0.5) and in both tumor models animals were monitored bi-weekly for bioluminescence to quantify tumor growth (40). See Supplementary preclinical methodology section for more details.

Mathematical Methodology: Fit procedures

Preclinical data: primary tumor and metastatic burden dynamics

Three fit procedures were investigated: 1) fitting the population average time series, 2) individual fits of each mouse's primary tumor (PT) and metastatic burden (MB) kinetics and 3) a mixed-effect population approach. Due to the high variability in the data, the first approach was not considered relevant. The second approach showed that the model was able to describe individual dynamics but, due to the relative scarcity of the data in a given animal, led to very poor identifiability of the coefficients, in particular the metastatic dissemination parameter μ. The third approach was considered the most appropriate to our case. Indeed, nonlinear mixed-effect modeling (41) is a statistical technique specifically tailored for sparse serial measurements in a population. It assumes that inter-animal variability can be

described by a parametric distribution on the model's parameters (here assumed to be lognormal, consistently with other works (20,42)). Multiple strategies were tested in order to find the appropriate formalism to fit the data. These included fitting PT and MB separately or together. The strategy fitting PT and MB was ultimately selected because it resulted in more accurate fits and allowed for possible correlations between the primary and secondary tumors growth parameters in a same animal.

One of the model parameters for Gomp-Exp growth was the *in vitro* proliferation rate, which was determined by an exponential fit to an *in vitro* proliferation assay. Maximization of the likelihood function under nonlinear mixed-effect formalism was solved using the function *nlmefitsa* implemented in Matlab (43), which is based on the stochastic approximation of expectation maximization (SAEM) algorithm. Specific assumptions were: log-transformation of the parameters (i.e. log-normal population distribution), proportional error model and full covariance matrix. For individual fits, weighted least squares minimization corresponding to individual likelihood maximization was performed using the function *fminsearch* of Matlab (Nelder-Mead algorithm), following previously reported methods (33).

Clinical data: Calculation of metastatic relapse probability

Our methodology for fitting the clinical data followed the same format as (44), although here the model was simplified (only parameter μ was allowed to vary among individuals) and PT size at diagnosis was considered to be uniformly distributed within each size range. Parameters for the growth of the primary and secondary tumors were fixed (not subject to optimization) and corresponded to a maximal volume of 10^{12} cells ($\simeq$ 1 kg) and a doubling time of 7.5 months at 1 g, consistently with clinical values reported in the literature (8,25).

The data reported in (26) consisted of metastatic relapse probabilities during the next 20 years post-surgery, for patients stratified by PT size (see Table 1). Diameter data from PT sizes at diagnosis were converted into volumes under the assumption of

a spherical shape and then converted to number of cells using the conversion rule 1 $mm^3 \simeq 10^6$ cells (45). Parameter μ was assumed log-normally distributed in the population, with mean μ^m and standard deviation μ^σ.

The probability of having a metastatic relapse in the next 20 years for a primary tumor diagnosed with a given size was assumed to be equal to the probability of already having one distant tumor at the time of diagnosis. For a given volume range of PT sizes at diagnosis $\left(V^k, V^{k+1}\right)$, $k \in \{1, \cdots, 7\}$, we considered the diagnosis volume V_D^k as a random variable uniformly distributed in $\left(V^k, V^{k+1}\right)$. Then, we computed the corresponding age of the tumor at diagnosis (i.e. the time elapsed from the first cancer cell) from the assumption of Gompertzian growth with the parameter values previously mentioned. This quantity was denoted $T_D(V_D^k)$. Under our formalism, the probability of having a disseminated metastasis at time $T_D(V_D^k)$ then writes

$$\mathbb{P}\left(\mathrm{Met}^k; \mu^m, \mu^\sigma\right) = \mathbb{P}\left(\mu \int_0^{T_D(V_D^k)} V_p(t)dt > 1\right) \quad (6)$$

where Met^k stands for the event of having one metastasis at diagnosis when the PT volume is in $\left(V^k, V^{k+1}\right)$. For any volume range and value of μ^m and μ^σ, this formalism allowed us to compute a probability to be compared to the respective empirical proportion of relapsing patients reported in (26), by simulating the two random variables involved (V_D^k and μ). We then determined the best-fit parameters by minimizing the sum of squared errors to the data, using the function *fminsearch* from Matlab.

Results

Quantitative and differential modeling of metastasis in ortho-surgical models

To mimic clinical progression of spontaneous systemic metastatic disease, two models involving orthotopic tumor implantation and surgical resection (ortho-surgical) were employed. These included a xenograft breast model (LM2-4^{LUC+} cells implanted into the mammary fat pad) and an isograft kidney model (RENCA^{LUC+} implanted into the subcapsular kidney space) (38) (see Methods). Presurgical primary tumor (PT) and postsurgical metastatic burden (MB) were tracked by bioluminescence (BL) emission, expressed in photons/second (p/s) (Figure 2A).

In the breast model, simultaneous BL and gross tumor volume measurements (caliper) were performed. The former only quantifies living cells whereas the latter computes a total volume indifferently of its composition. Volume and BL emission were significantly correlated (supplementary Figure 1B), as observed by others (46). Determination of the signal corresponding to one cell was required in our modeling for the value assigned to V_0. Based on linear regression between BL emission and tumor volume, we established that BL = $2.19 \cdot 10^6$ V + $7.89 \cdot 10^7$, where BL is the bioluminescence in p/s and V is the volume in mm^3. This relationship, evaluated at V = 10 mm^3 ≃ 10^7 cells gives 1 cell ≃ 10.08 p/s, which was approximated to 10 p/s. Using this value gave reasonable fits to the PT growth data (supplementary Figure 2).

Validation and calibration of the mathematical model

We assessed the ability of the models to describe and predict the experimental data of postsurgical MB dynamics. Several model designs were evaluated to define the optimal structure and methodology that would allow accurate and reliable data description. Specifically, for each *in vivo* experimental system, multiple structural expressions and parametric dependences between the growth rate of the PT and MB

were tested. We refer to supplementary Figures 3 and 4 for direct comparison of goodness-of-fit and identifiability under different modeling setups. Population and individual fits of the best models to the data are shown in Figures 2B-C (and supplementary Figure 5), and Figure 3, respectively. The parameter values inferred from the population fits are reported in Table 2. The mathematical models – combined with the population distribution of the parameters inferred from the nonlinear mixed-effects statistical procedure – were able to give reasonable descriptions of the presurgical PT and postsurgical MB growth. Importantly, these combinations could quantify the dynamics of the process as well as the inter-animal variability. The latter was better characterized by the metastatic potential parameter μ (large coefficients of variation in Table 2). The models could also fit individual dynamics of longitudinal data of pre-surgical PT and post-surgical MB (see Figure 3 for some representative examples of growth dynamics in particular mice and supplementary Figures 6 and 7 for fits of all mice).

In addition to their descriptive power, the models were able to predict growth dynamics in external data sets that were not employed for estimation of the parameters (Figure 2D-E). These results emphasize the ability of our general modeling structure to capture MB growth dynamics. Additionally, the modeled post-surgical MB could also be related to empirical survival by means of a lethal burden threshold, which was estimated to be 4×10^9 p/s (supplementary Figure 8).

Qualitative and quantitative differences across ortho-surgical models

Xenograft Model: Breast metastasis

Using the same growth model (Gomp-Exp) and parameters for both presurgical PT and postsurgical MB, we were able to adequately fit the data, while ensuring reasonable standard errors on the parameters estimates (Table 2). Although more complex structures (e.g. models with one parameter differing between primary and secondary growth) provided marginally better fits, robustness in estimating μ was

impaired (supplementary Figure 3). Quantitative inference of μ revealed small metastatic potential (Table 2), which translated into late development of metastases following xenograft and growth of the MB mostly dominated by proliferation (Figures 2B, 3A-C).

Isograft Model: Kidney metastasis

In contrast, the kidney model MB growth curves exhibited a different behavior, with a marked change of regimen at the time of surgery. In the context of the model, this means that most of the presurgical MB increase was driven by the dissemination process, and not by proliferation of the metastases themselves. This was reflected by a very large value of μ (Table 2), with nine orders of magnitude of difference compared to the breast model. This feature was not directly visible, nor quantifiable, by direct examination of the data, and reflects the large metastatic aggressiveness of isograft spontaneous metastasis animal models, since overpassing the immune surveillance is a major challenge in the metastatic process (4). When the PT was removed, dissemination stopped and only proliferation remained for further growth of the MB, which happened at a slower rate than at the primary site (Figures 2C and 3D-F). In some cases, growth of the MB remained constant or even decreased after surgery (see supplementary Figure 7). This result reflects the fact that the competent immune status of the mice might have an important impact on the establishment of durable, fast-growing metastatic colonies at the secondary sites (47).

Together, our data-based quantitative modeling analysis of presurgical PT and postsurgical MB growth kinetics demonstrated the descriptive power of the models, unraveled distinct growth patterns between the two animal models and emphasized the critical role of the parameter μ for quantification of the inter-animal variability.

Clinical data of metastatic relapse probability

Clinical data reported in the literature generally do not provide detailed information about the untreated growth of the metastatic burden, either because the residual

disease is invisible, or because the patients benefit from adjuvant therapy after resection of their PT. Nevertheless, before the generalization of adjuvant therapy for breast cancer, Koscielny et al. (26) reported data from a cohort of 2648 patients followed for 20 years after surgery of the PT, without additional treatment. Their data (reproduced in Table 1) demonstrated that, despite a clear association between PT size at diagnosis and the probability of metastatic relapse, not all the patients having a given PT size were relapsing. For instance, only 42% of patients with a PT diameter at diagnosis between 2.5 and 3.5 centimeters developed metastasis. Based on this observation, we used our model to describe inter-individual variability by means of a limited number of parameters. We considered that the probability of developing a metastasis in the next 20 years was equal to the probability of already having one at the time of diagnosis (see Methods). Using a lognormal population distribution of parameter μ we were able to obtain a significant fit to the data of metastatic relapse for all size ranges (Table 1, p = 0.023). Interestingly, the median value of μ resulting from these human data was close to the value from the preclinical breast data, in comparison to the kidney model.

These results demonstrated that, within our semi-mechanistic modeling approach, parameter μ was able to capture the inter-individual metastatic variability, not only in animal models, but also for patient data.

Assessing the impact of surgery on metastasis and survival: a simulation study

When diagnosis detects only a localized primary tumor, distant occult disease might already be present. In our model, the extent of this invisible metastatic burden depends on: 1) the PT size at diagnosis and 2) the patient's metastatic potential μ. For instance, if the PT size (or μ) is small then the occult MB might be negligible and surgery would substantially benefit to the patient in terms of metastatic reduction, by stopping further spread of new foci. Conversely, if the PT size (or μ) is large, then the

occult MB might already be consequent and removing the PT might only have a marginal impact.

Virtual simulation of two breast cancer patients

We simulated the quantitative impact of PT surgery in two virtual breast cancer patients having a PT diagnosed at 4.32 cm and two values of μ (median and 90th percentile within a population distributed according to our previous estimate). Results are reported in Figure 4 and supplementary movies 1 and 2. A discrete and stochastic version of the metastatic dissemination was employed here for the simulations (see supplementary methods for details). Interestingly, our simulation revealed that at the time of diagnosis, no metastasis was detectable (i.e. below the imaging detection limit, taken here to 10^8 cells), in both cases (Figure 4A-B). In clinical terms, this means that both patients would have been diagnosed with a localized disease. However, the two size distributions were very different, with a much larger residual burden in the "large μ" case, illustrative of the increased metastatic potential.

For the "median μ" case, our model predicted the presence of two small metastases, with respective sizes 6 and 278 cells. Not surprisingly, when no surgery was simulated, this number continued to increase, reaching 160 secondary lesions after 15 years (Figure 4C). However, most of the metastatic burden (126 tumors, i.e. 78.8% of the total burden) was composed of lesions smaller than 10^9 cells ($\simeq$1g). Panels E and G of Figure 4 demonstrate that a substantial relative benefit (larger than 10%) in MB reduction was eventually obtained, but only after 7.8 years. Nevertheless, at the end of the simulation (15 years after surgery), the predicted two occult metastases at diagnosis had reached substantial sizes (1.41×10^{11} and 1.89×10^{11} cells). Therefore, for this patient with median metastatic potential, the model indicates an important benefit in using adjuvant therapy.

For a patient with higher metastatic potential (at the level of the 90th percentile, see Figure 4 panels B, D, F and H, and supplementary movie 2), even with a PT

diagnosed at the same size, the predicted metastatic burden at diagnosis was considerably more important, with 76 lesions and the largest comprising 6.23×10^6 cells. This consequent occult burden translated into poor outcome and the metastatic mass would have reached a lethal burden of 10^{12} cells 9.3 years after the initial diagnosis if no therapy would have been administrated.

These results illustrate the potential of the model as a diagnosis and prognosis numerical tool for assessment of the occult metastatic burden and post-surgery growth. In this, it could help to determine the extent of adjuvant therapy necessary to achieve a long-term control of the disease.

Impact of tumor size on postsurgical survival

To further examine the relationship between the PT size at surgery and survival, we performed simulations for 1) an individual with fixed value of μ (the population median, see Figure 5A) or 2) an entire population (simulated survival curves in Figure 5B), for three PT sizes. Numerical survival was defined by the time to reach a lethal burden of 1 kg ($\simeq 10^{12}$ cells) (2) from the time of cancer inception. Interestingly, we observed a highly nonlinear relationship between the PT size and the survival, which suggested three size ranges delimited by two thresholds (Figure 5A). The lower threshold — termed 'recurrence' threshold (4 cm in Figure 5A) — was defined as the maximal limit whereupon no metastasis was present at surgery (number of metastases lower than 1). The upper size threshold — termed 'benefit' threshold (5.2 cm in Figure 5A) — was defined as the size above which surgery had a negligible (< 10%) impact on survival time. Above and below these 'recurrence' and 'benefit' thresholds, PT size had no important correlative value. Conversely, within the PT size range delimited by these two bounds, the relationship between presurgical PT and postsurgical MB/survival was highly correlative, with a large derivative and a sharp transition between the two extremes. The same qualitative PT size/survival

relationship was obtained for any value of μ sampled within the population distribution (see supplementary Figure 9).

In Figure 5C, we present quantitative estimates of the recurrence and benefit thresholds for various percentiles of μ within the population distribution (see also supplementary Figure 9). Our simulations predicted that for the first half of the population, surgery was almost always leading to negligible metastatic recurrence risk, with large values of the recurrence threshold (larger than the usual detection levels). On the other hand, the patients with large metastatic potential were predicted not to substantially benefit from the surgery, as far as reduction of future MB was concerned. For instance, a patient with μ at the level of the 90^{th} percentile and a PT diagnosed at 4 cm would have an increase in absolute survival time of only 1.9% following surgery (Figure 5C).

Discussion

Using a formalism based on simple laws of metastatic development (including dissemination and proliferation), we derived mathematical models able to connect presurgical PT growth to postsurgical development of the MB in two ortho-surgical animal models (with two immune states) as well as one clinical data set. These quantitative models allowed identification of different metastatic growth patterns and characterization of the metastatic potential (and associated inter-animal/individual variability) as a critical parameter, μ. Our results also revealed a nonlinear quantitative relationship between the PT size at diagnosis and post-surgical survival improvement.

Previous studies have utilized experimental data derived from mouse metastasis models to inform mathematical analysis. For instance, Hartung and colleagues used human MDA-MB-231 breast cancer cells implanted orthotopically in mice in order to validate a mathematical model for longitudinal data of metastatic burden growth (21). This animal model was non-surgical and utilized severe immunocompromised Nod SCID γ mice to improve the low metastatic potential observed in the MDA-MB-231, a phenomena recently reported elsewhere (47). In our studies, we utilized a variant of the MDA-MB-231 previously selected for increased metastatic potential by repeated orthotopic implantation and metastatic resection in SCID mice (36). Since the selection of cells and immune state could influence analysis, we also included an immunocompetent mouse kidney model to confirm (and compare) findings. While these and other modifications to the metastatic systems could significantly influence mathematical modeling (i.e., different mouse strain and cell line, different bioluminescence technique, etc…), the impact of surgery appears to be the most

significant factor. In this regard, several technical discrepancies likely impair a relevant comparison between surgical and non-surgical models presented by Hartung, et al. (21) and the current study. For instance, in surgical models we found it unnecessary to assume different growth between the primary and secondary lesions in surgical models. Additionally, we considered a less complex dissemination rate (expression $d(V_p) = \mu V_p^{\gamma}$ and $\gamma = \frac{2}{3}$ was used in (21)). Notably, we could fit our data equally well with various values of γ and thus concluded that it cannot be identified from combined PT growth and MB dynamics data alone (supplementary Figure 10). Future studies would require more data, especially on the number and size distribution of the secondary lesions, to precisely determine the shape of the dissemination coefficient. When using the dissemination and growth terms from (21) and fitting the resulting model to our surgical data, we found a much larger metastatic potential μ and a significantly faster metastatic growth kinetics parameter than computed in the non-surgical model (21) (see supplementary text). While the former probably illustrates higher metastatic propensity due to a more permissive immune state, the latter possibly suggests post-surgery metastatic acceleration (48-50).

In this regard, this raises another critical consideration of the impact of surgery on metastatic potential in mathematical modeling. Preclinical and clinical works have suggested that removal of the PT might provoke acceleration of metastatic growth (50,52). There are various biological rationales that could explain this, including inhibition of secondary growth by the presence of a primary neoplasm as a result of nutrient availability, concomitant immunity, or even systemic inhibition of angiogenesis (53). Such a theory could conceivably be assessed within the context of our model by defining different pre- and post-surgical metastatic growth rates $g(v)$ and comparing

goodness of fit. However, this would add at least one degree of freedom (thus deteriorating the reliability of the estimation) and invalidate the convolution formula used for computation of the metastatic burden in a model with non-autonomous $g(t,v)$ (instead of $g(v)$), and therefore was not considered here. Importantly, theoretical integration of higher order phenomena for the biological dynamics of metastatic development has been considered elsewhere (14,16,18,54) and recent findings in the organism-scale dynamics of metastases (such as the self-seeding phenomenon (5,6) or the influence of the (pre-) metastatic niche (55)) could be embedded within the general formalism developed in our model. This could lead to complex models, however, and given the amount of information contained in our present data, reliable identification of such dynamics was not realistic. Instead, we only considered metastatic dynamics as reduced to its most essential features: dissemination and proliferation. Future studies should examine the potential of metastases to metastasize, as has been extensively debated in the past (56-58), particularly with the recent demonstration that some metastases are able to re-seed the primary tumor (5,6). Although not included in this study, preliminary tests using our model suggest negligible differences in the simulations and no impact on our results, however a more extensive analysis is required.

Our modeling philosophy elaborates on Fisher's theory (59) of cancer as a systemic disease and relates also to the parallel progression model (2). The dissemination rate d, characterized by parameter μ, quantifies the metastatic potential and allows for a *continuum* of possibilities between early and late dissemination. Our results seem to parallel clinical evidence of the impact (and importance) of early surgery – particularly in the case of breast cancer. For example, in a retrospective study of 2838 breast cancer patients, the post-surgical residual recurrence-free

survival rate at 5 years for Stage I disease was 7% (60). Consistently, our quantitative analysis demonstrates that in this case, for most patients, metastases that could have been shed before diagnosis would not develop into overt clinical disease during the remaining life history of the patient. For Stage IV breast cancer (that would correspond, in our formalism, to a large value of μ), our analysis predicts only negligible benefit of the surgery (if only considering reduction of metastatic shedding), in accordance with preliminary results of a recent clinical trial (61). In order to use our model as a practical diagnosis and prognosis tool that could help to refine and individualize adjuvant therapy, the critical next step is to find a way to estimate the parameter μ, in a patient-specific manner. One of the main challenges will be to do so using data derived from the primary tumor only, since metastases are often undetectable at the time of diagnosis. While the value of μ might very likely depend on the combination of several phenomena (including some genetic alterations or the immune status of the patient which could be linked to different biomarkers (62)), recent successes of genetic signatures as prognosis factors for metastasis might allow for patient-specific estimation of μ (63).

Any mathematical modeling attempt is limited by the intrinsic measurement error of the experimental technique. For monitoring the dynamics of total metastatic burden, bioluminescence imaging represents one of the best methods so far (51). However, measurement variability is hard to assess due to inherent issues, such as the long half-life of luciferin that prevents immediate replication of the measurements. Comparison of bioluminescence with caliper measurements showed large variance (supplementary Figure 1B), which increased with tumor size. This justified our assumption of a proportional measurement error model. Standard deviation of the relative error could in turn be estimated from the fit procedure and yielded a value of

0.72. This high degree of uncertainty should be taken into account as an inevitable limitation for quantitative modeling studies of bioluminescence data. We therefore put a strong emphasis on using a minimal number of parameters and assessed the robustness of our results on various assumptions, such as the shape of d and the value of V_0 (supplementary Figures 10 and 11).

Together, our mathematical methodology provides a quantitative *in silico* framework that could be of valuable help for preclinical and clinical aims. Indeed, validation of our modeling methodology allows us to address in future works the differential effects of systemic therapies on primary tumor growth and metastases (39,40). Clinically, our methodology could be used to refine/optimize therapeutic strategies for patients diagnosed with a localized cancer and inform on the timing of surgery, extent of occult metastatic disease and probability of recurrence. In turn, this may impact decisions on duration and intensity of presurgical neoadjuvant or postsurgical adjuvant treatments (64).

Acknowledgements

This study has been carried out within the frame of the LABEX TRAIL, ANR-10-LABX-0057 with financial support from the French State, managed by the French National Research Agency (ANR) in the frame of the « Investments for the future » Programme IdEx (ANR-10-IDEX-03-02). This work was also supported by Roswell Park Alliance Foundation (RPAF) and by the Department of Defense (DoD), through the Peer Reviewed Cancer Research Program, under Award No. W81XWH-14-1-0210 (both to JMLE).

Disclaimer

Opinions, interpretations, conclusions and recommendations are those of the authors and are not necessarily endorsed by the RPAF or DoD.

References

1. Gupta GP, Massagué J. Cancer metastasis: building a framework. Cell. 2006;127:679–95.

2. Klein CA. Parallel progression of primary tumours and metastases. Nat Rev Cancer. 2009;9:302–12.

3. Hanahan D, Weinberg RA. The hallmarks of cancer. Cell. 2000;100:57–70.

4. Hanahan D, Weinberg RA. Hallmarks of cancer: the next generation. Cell. 2011;144:646–74.

5. Comen E, Norton L, Massagué J. Clinical implications of cancer self-seeding. Nat Rev Clin Oncol. 2011;8:369–77.

6. Kim M-Y, Oskarsson T, Acharyya S, Nguyen DX, Zhang XHF, Norton L, et al. Tumor self-seeding by circulating cancer cells. Cell. 2009;139:1315–26.

7. Slack NH, Blumenson LE, Bross ID. Therapeutic implications from a mathematical model characterizing the course of breast cancer. Cancer. 1969;24:960–71.

8. Koscielny S, Tubiana M, Valleron AJ. A simulation model of the natural history of human breast cancer. Br J Cancer. 1985;52:515–24.

9. Liotta LA, Saidel GM, Kleinerman J. Stochastic model of metastases formation. Biometrics. 1976;32:535–50.

10. Iwata K, Kawasaki K, Shigesada N. A Dynamical Model for the Growth and Size Distribution of Multiple Metastatic Tumors. J Theor Biol. 2000;203:177–86.

11. Hahnfeldt P, Panigrahy D, Folkman J, Hlatky L. Tumor development under angiogenic signaling: a dynamical theory of tumor growth, treatment response, and postvascular dormancy. Cancer Res. 1999;59:4770–5.

12. Michor F. Mathematical models of cancer stem cells. J Clin Oncol. 2008;26:2854–61.

13. Wilkie KP, Hahnfeldt P. Tumor-immune dynamics regulated in the microenvironment inform the transient nature of immune-induced tumor dormancy. Cancer Res. 2013;73:3534–44.

14. Kim Y, Boushaba K. Regulation of tumor dormancy and role of microenvironment: a mathematical model. Advances Exp Med Biol. 2013;734:237–59.

15. Michor F, Nowak MA, Iwasa Y. Stochastic dynamics of metastasis formation. J

Theor Biol. 2006;240:521–30.

16. Diego D, Calvo GF, Pérez-García VM. Modeling the connection between primary and metastatic tumors. J Math Biol. 2013;67:657–92.

17. Bartoszyński R. A modeling approach to metastatic progression of cancer. In: Thompson JR, Brown BW, editors. Cancer Modeling. 1987. pages 237–67.

18. Hanin L. Seeing the invisible: how mathematical models uncover tumor dormancy, reconstruct the natural history of cancer, and assess the effects of treatment. Advances Exp Med Biol. 2013;734:261–82.

19. Retsky MW, Demicheli R, Swartzendruber DE, Bame PD, Wardwell RH, Bonadonna G, et al. Computer simulation of a breast cancer metastasis model. Breast Cancer Res Treat. 1997;45:193–202.

20. Yorke ED, Fuks Z, Norton L, Whitmore W, Ling CC. Modeling the development of metastases from primary and locally recurrent tumors: comparison with a clinical data base for prostatic cancer. Cancer Res. 1993;53:2987–93.

21. Hartung N, Mollard S, Barbolosi D, Benabdallah A, Chapuisat G, Henry G, et al. Mathematical modeling of tumor growth and metastatic spreading: validation in tumor-bearing mice. Cancer Res. 2014;74:6397–407.

22. Haeno H, Gonen M, Davis MB, Herman JM, Iacobuzio-Donahue CA, Michor F. Computational Modeling of Pancreatic Cancer Reveals Kinetics of Metastasis Suggesting Optimum Treatment Strategies. Cell. 2012;148:362–75.

23. Francia G, Cruz-Munoz W, Man S, Xu P, Kerbel RS. Mouse models of advanced spontaneous metastasis for experimental therapeutics. Nat Rev Cancer. 2011;11:135–41.

24. Talmadge JE, Singh RK, Fidler IJ, Raz A. Murine models to evaluate novel and conventional therapeutic strategies for cancer. Am J Pathol. 2007;170:793–804.

25. Coumans FAW, Siesling S, Terstappen LWMM. Detection of cancer before distant metastasis. BMC Cancer. 2013;13:283.

26. Koscielny S, Tubiana M, Le MG, Valleron A, Mouriesse H, Contesso G, et al. Breast cancer: relationship between the size of the primary tumour and the probability of metastatic dissemination. Br J Cancer. 1984;49:709–15.

27. McMillin DW, Negri JM, Mitsiades CS. The role of tumour-stromal interactions in modifying drug response: challenges and opportunities. Nat Rev Drug Discov. 2013;12:217–28.

28. Benzekry S, André N, Benabdallah A, Ciccolini J, Faivre C, Hubert F, et al. Modelling the impact of anticancer agents on metastatic spreading. Math Model Nat Phenom. 2012;7:306–36.

29. Benzekry S, Hahnfeldt P. Maximum tolerated dose versus metronomic scheduling in the treatment of metastatic cancers. J Theor Biol. 2013;335:235–44.

30. Talmadge JE, Fidler IJ. AACR centennial series: the biology of cancer metastasis: historical perspective. Cancer Res. 2010;70:5649–69.

31. Scott JG, Gerlee P, Basanta D, Fletcher AG. Mathematical modeling of the metastatic process. In: Malek A, editor. Experimental Metastasis: Modeling and Analysis. 2013.

32. Wheldon TE. Mathematical models in cancer research. 1988.

33. Benzekry S, Lamont C, Beheshti A, Tracz A, Ebos JML, Hlatky L, et al. Classical mathematical models for description and prediction of experimental tumor growth. PLoS Comput Biol. 2014;10:e1003800.

34. Steel GG, Lamerton LF. The growth rate of human tumours. Br J Cancer. 1966;20:74–86.

35. Hartung N. Efficient resolution of metastatic tumor growth models by reformulation into integral equations. Discrete Contin Dyn Syst Ser B. 2015;20:445–67.

36. Munoz R, Man S, Shaked Y, Lee CR, Wong J, Francia G, et al. Highly efficacious nontoxic preclinical treatment for advanced metastatic breast cancer using combination oral UFT-cyclophosphamide metronomic chemotherapy. Cancer Res. 2006;66:3386–91.

37. Ebos JML, Lee CR, Bogdanovic E, Alami J, Van Slyke P, Francia G, et al. Vascular endothelial growth factor-mediated decrease in plasma soluble vascular endothelial growth factor receptor-2 levels as a surrogate biomarker for tumor growth. Cancer Res. 2008;68:521–9.

38. Tracz A, Mastri M, Lee CR, Pili R, Ebos JML. Modeling spontaneous metastatic renal cell carcinoma (mRCC) in mice following nephrectomy. J Vis Exp. 2014;:e51485–5.

39. Ebos JML, Mastri M, Lee CR, Tracz A, Hudson JM, Attwood K, et al. Neoadjuvant antiangiogenic therapy reveals contrasts in primary and metastatic tumor efficacy. EMBO Mol Med. 2014;6:1561–76.

40. Ebos JML, Lee CR, Cruz-Munoz W, Bjarnason GA, Christensen JG, Kerbel RS. Accelerated metastasis after short-term treatment with a potent inhibitor of tumor angiogenesis. Cancer Cell. 2009;15:232–9.

41. Lavielle M. Mixed Effects Models for the Population Approach. 2014.

42. Norton L. A Gompertzian model of human breast cancer growth. Cancer Res. 1988;48:7067–71.

43. Mathworks T. Matlab with statistics and optimization toolboxes. 2013.

44. Barbolosi D, Verga F, You B, Benabdallah A, Hubert F, Mercier C, et al. Modélisation du risque d'évolution métastatique chez les patients supposés avoir une maladie localisée. Oncologie. 2011;13:528–33.

45. Spratt JS, Meyer JS, Spratt JA. Rates of growth of human solid neoplasms: Part I. J Surg Oncol. 1995;60:137–46.

46. Shan L, Wang S, Korotcov A, Sridhar R, Wang PC. Bioluminescent animal models of human breast cancer for tumor biomass evaluation and metastasis detection. Ethn Dis. 2008;18:S2–65–S2–69.

47. Milsom CC, Lee CR, Hackl C, Man S, Kerbel RS. Differential post-surgical metastasis and survival in SCID, NOD-SCID and NOD-SCID-IL-2Rγ(null) mice with parental and subline variants of human breast cancer: implications for host defense mechanisms regulating metastasis. PLoS ONE. 2013;8:e71270.

48. Demicheli R, Retsky MW, Hrushesky WJM, Baum M, Gukas ID. The effects of surgery on tumor growth: a century of investigations. Ann Oncol. 2008;19:1821–8.

49. Demicheli R, Retsky MW, Hrushesky WJM, Baum M. Tumor dormancy and surgery-driven interruption of dormancy in breast cancer: learning from failures. Nat Clin Rev Oncol. 2007;4:699–710.

50. Coffey JC, Wang JH, Smith MJF, Bouchier-Hayes D, Cotter TG, Redmond HP. Excisional surgery for cancer cure: therapy at a cost. Lancet Oncology. 2003;4:760–8.

51. Neill KO, Lyons SK, Gallagher WM, Curran KM, Byrne AT. Bioluminescent imaging : a critical tool in pre-clinical oncology research. J Pathol. 2010;220:317–27.

52. Retsky M, Demicheli R, Hrushesky W, Baum M, Gukas I. Surgery triggers outgrowth of latent distant disease in breast cancer: an inconvenient truth? Cancers. 2010;2:305–37.

53. Chiarella P, Bruzzo J, Meiss RP, Ruggiero RA. Concomitant tumor resistance. Cancer Lett. 2012;324:133–41.

54. Benzekry S, Gandolfi A, Hahnfeldt P. Global Dormancy of Metastases Due to Systemic Inhibition of Angiogenesis. PLoS ONE. 2014;9:e84249–11.

55. Peinado H, Lavotshkin S, Lyden D. The secreted factors responsible for pre-metastatic niche formation: old sayings and new thoughts. Semin Cancer Biol. 2011;21:139–46.

56. Tait CR, Dodwell D, Horgan K. Do metastases metastasize? J Pathol. 2004;203:515–8.

57. Sugarbaker EV, Cohen AM, Ketcham AS. Do metastases metastasize? Annals of surgery. 1971;174:161–6.

58. Bethge A, Schumacher U, Wree A, Wedemann G. Are metastases from metastases clinical relevant? Computer modelling of cancer spread in a case of hepatocellular carcinoma. PLoS ONE. 2012;7:e35689–9.

59. Fisher B. Biological and clinical considerations regarding the use of surgery and chemotherapy in the treatment of primary breast cancer. Cancer. 1977;40:574–87.

60. Brewster AM, Hortobagyi GN, Broglio KR, Kau S-W, Santa-Maria CA, Arun B, et al. Residual risk of breast cancer recurrence 5 years after adjuvant therapy. JNCI Journal of the National Cancer Institute. 2008;100:1179–83.

61. Badwe R, Parmar V, Hawaldar R, Nair N, Kaushik R, Siddique S, et al. Surgical removal of primary tumor and axillary lymph nodes in women with metastatic breast cancer at first presentation: A randomized controlled trial. San Antonio Breast Cancer Symposium. 2013. pages S2–02.

62. Di Gioia D, Stieber P, Schmidt GP, Nagel D, Heinemann V, Baur-Melnyk A. Early detection of metastatic disease in asymptomatic breast cancer patients with whole-body imaging and defined tumour marker increase. Br J Cancer. 2015;112:809–18.

63. Reis-Filho JS, Pusztai L. Gene expression profiling in breast cancer: classification, prognostication, and prediction. Lancet. 2011;378:1812–23.

64. Early Breast Cancer Trialists' Collaborative Group (EBCTCG). Effects of chemotherapy and hormonal therapy for early breast cancer on recurrence and 15-year survival: an overview of the randomised trials. Lancet. 2005;365:1687–717.

Figure 1

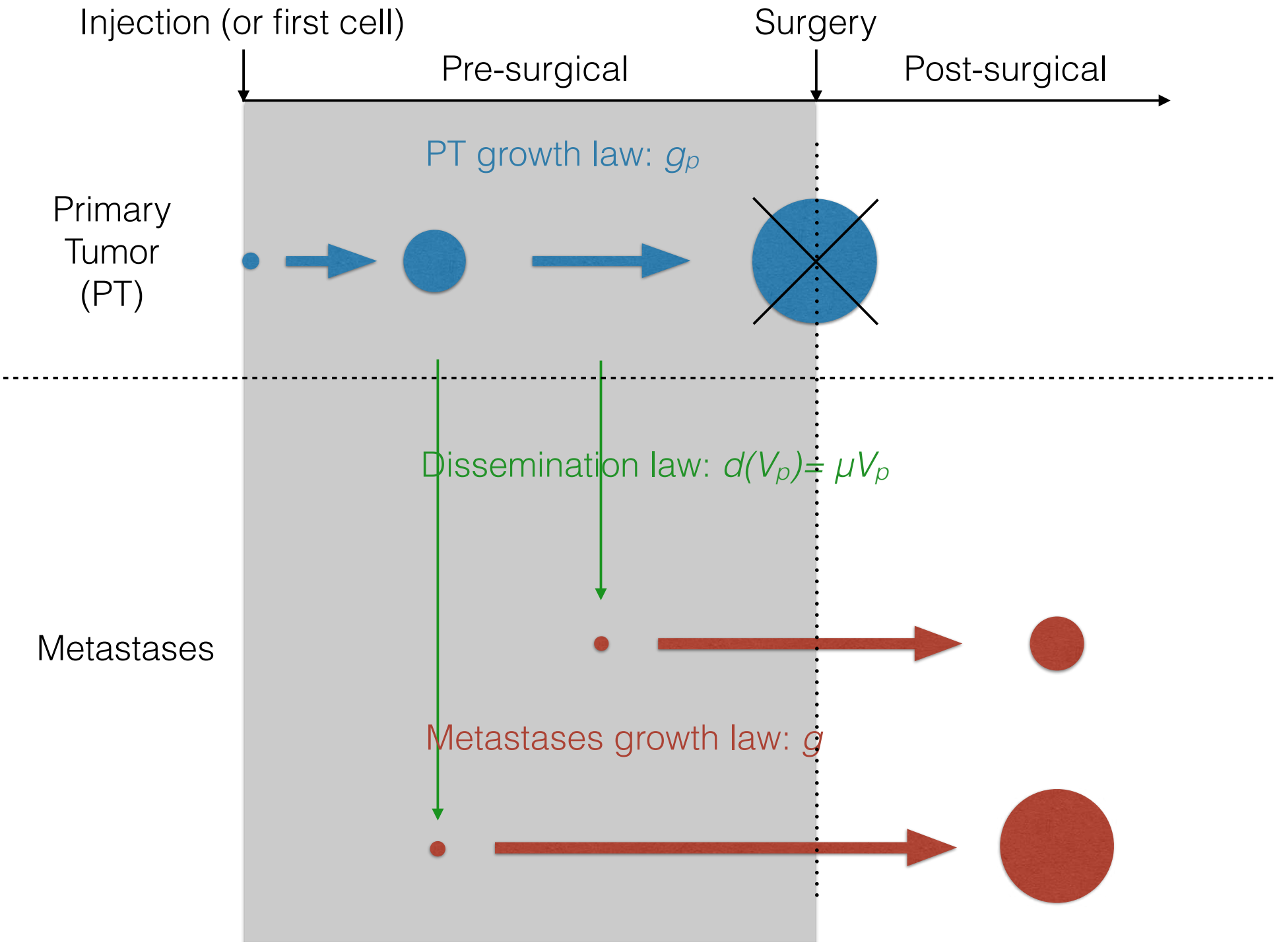
Injection (or first cell)
Surgery
Pre-surgical
Post-surgical
PT growth law: g_p
Primary Tumor (PT)
Dissemination law: $d(V_p) = \mu V_p$
Metastases
Metastases growth law: g

Figure 2

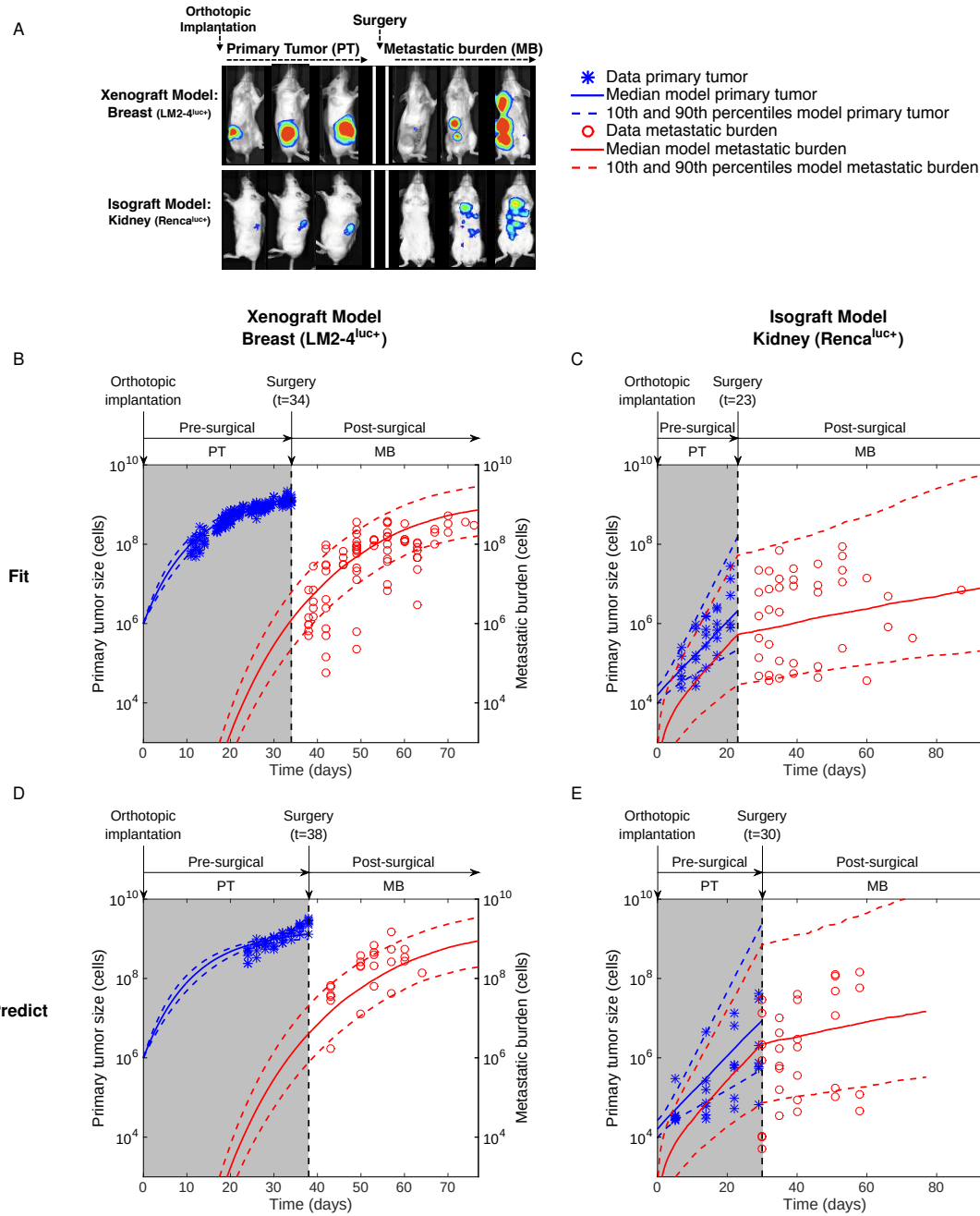
A
Orthotopic Implantation
Surgery
Primary Tumor (PT)
Metastatic burden (MB)
Xenograft Model: Breast (LM2-4luc+)
Isograft Model: Kidney (Rencaluc+)
Data primary tumor
Median model primary tumor
10th and 90th percentiles model primary tumor
Data metastatic burden
Median model metastatic burden
10th and 90th percentiles model metastatic burden
Xenograft Model Breast (LM2-4luc+)
Isograft Model Kidney (Rencaluc+)
B
C
Fit
Orthotopic implantation
Surgery (t=34)
Surgery (t=23)
Pre-surgical
Post-surgical
PT
MB
Primary tumor size (cells)
Metastatic burden (cells)
Time (days)
D
E
Predict
Surgery (t=38)
Surgery (t=30)

Figure 3

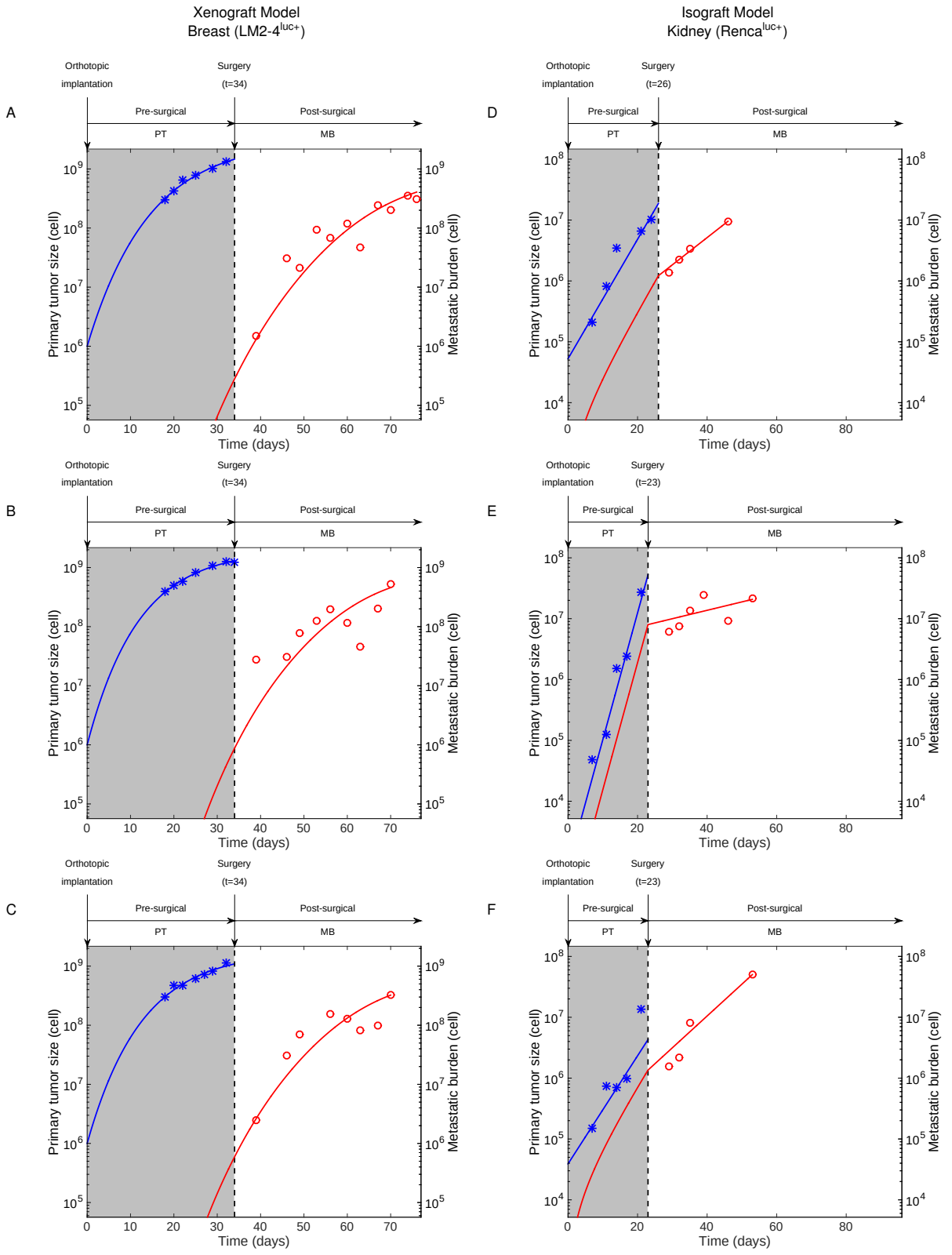
Xenograft Model
Breast (LM2-4luc+)
Isograft Model
Kidney (Renca luc+)
A
B
C
D
E
F
Orthotopic implantation
Surgery (t=34)
Surgery (t=26)
Surgery (t=23)
Pre-surgical
Post-surgical
PT
MB
Primary tumor size (cell)
Metastatic burden (cell)
Time (days)
Data primary tumor
Model primary tumor
Data metastatic burden
Model metastatic burden

Figure 4

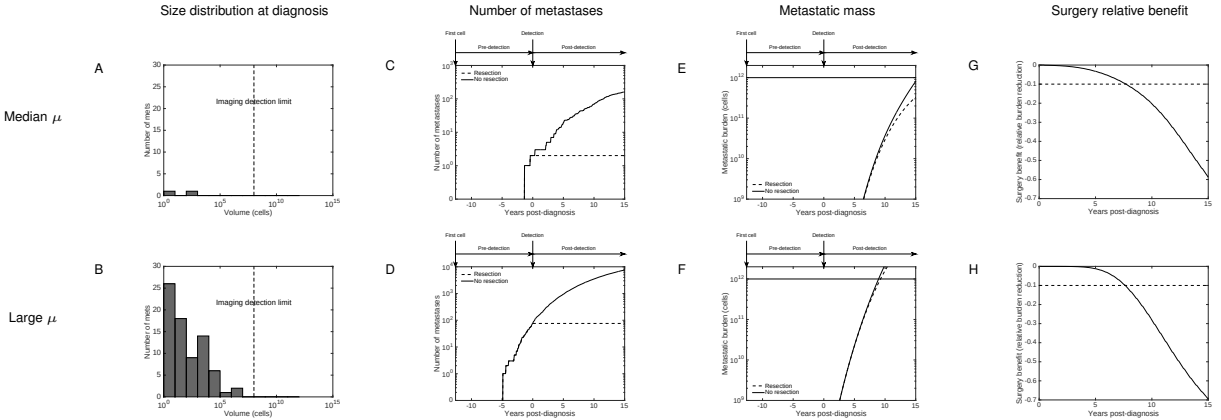
Size distribution at diagnosis
Number of metastases
Metastatic mass
Surgery relative benefit
Median μ
Large μ
A
B
C
D
E
F
G
H
Imaging detection limit
Number of mets
Volume (cells)
First cell
Detection
Pre-detection
Post-detection
Resection
No resection
Number of metastases
Metastatic burden (cells)
Years post-diagnosis
Surgery benefit (relative burden reduction)

Figure 5

A

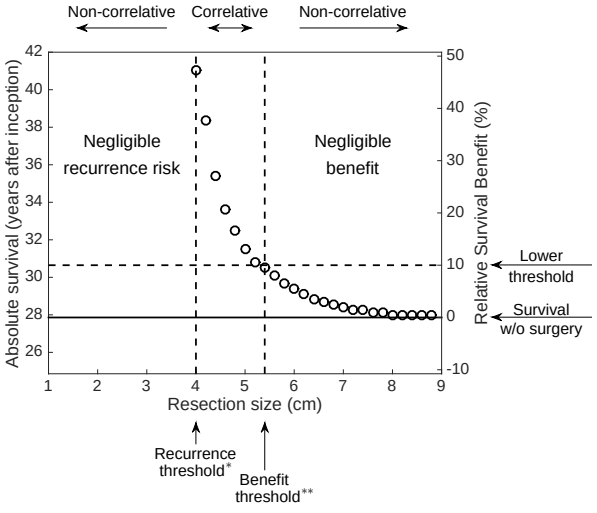

B

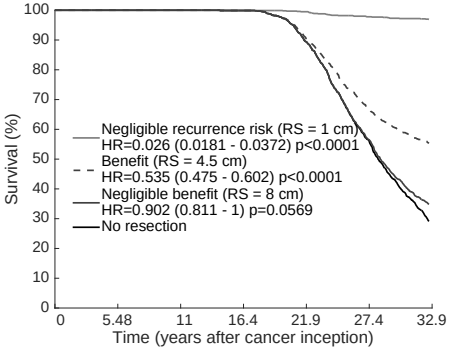

C

Percentile of μ	10	25	37.5	50	62.5	75	90
$RSB(\mu)$ (%)	∞	∞	∞	47	14	6.4	1.9
Recurrence threshold (cm)	-	6.6	5.2	4	3	2.4	1.4
Benefit threshold (cm)	-	7.8	6.4	5.4	4.6	3.6	2.6

D

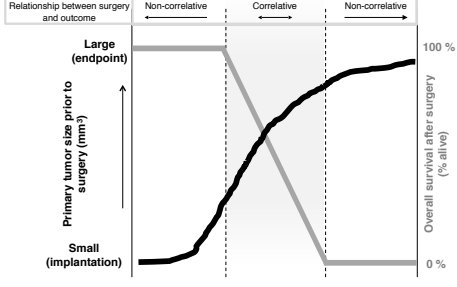

Table 1: Descriptive power of the mathematical model: clinical data of metastatic relapse probability

Diameter (cm)	No. patients	Prop. of relapse (Data)	Prop. of relapse (Model)
$1 \leq D \leq 2.5$	317	27.1	25.5
$2.5 < D \leq 3.5$	496	42.0	42.4
$3.5 < D \leq 4.5$	544	56.7	56.3
$4.5 < D \leq 5.5$	422	66.5	65.9
$5.5 < D \leq 6.5$	329	72.8	74.3
$6.5 < D \leq 7.5$	192	83.8	80.8
$7.5 < D \leq 8.5$	136	81.3	85.7

Fit of the model was significant for Pearson's χ^2 test for goodness-of-fit ($p = 0.023$).

Table 2: Parameters inferred from the models

Data	Growth model	Location	Par.	Unit	Estimate (CV)	95 % CI
In vitro (Breast)	Exp.		λ	day^{-1}	0.837 (-)	(0.795 - 0.879)
Preclinical Breast	Gomp-Exp.	PT	V_i	$cell$	1.00×10^6 (-)	-
			α	day^{-1}	1.9 (5.73)	(1.84 - 1.96)
			β	day^{-1}	0.0893 (21.3)	(0.0791 - 0.101)
		Met	V_0	p/s	10 (-)	-
			μ	$cell^{-1} \cdot day^{-1}$	4.43×10^{-11} (176)	$(2.70 \times 10^{-11}$ - $7.27 \times 10^{-11})$
Preclinical Kidney	Exp.	PT	V_i	p/s	1.63×10^5 (45.5)	$(9.40 \times 10^4$ - $2.83 \times 10^5)$
			α_p	day^{-1}	0.21 (60.3)	(0.151 - 0.292)
		Met	V_0	p/s	10 (-)	-
			α	day^{-1}	0.0307 (201)	(0.0133 - 0.0707)
			μ	$cell^{-1} \cdot day^{-1}$	0.0415 (397)	(0.0181 - 0.0948)
Clinical Breast	Gomp.	PT	V_i	$cell$	1 (-)	
			α	day^{-1}	0.013 (-)	
			β	day^{-1}	0.000471 (-)	
		Met	V_0	$cell$	1 (-)	
			μ	$cell^{-1} \cdot day^{-1}$	7.00×10^{-12} (1.04×10^4)	

Parameters corresponding to the preclinical data were obtained using nonlinear mixed-effects modeling. Inter-animal variability of each parameter is captured by its respective coefficient of variation (CV). Parameter values for the clinical data are those that produced the fit to the clinical data of metastatic relapse probability from (26), reported in Table 1. For these data, only parameter μ was allowed to vary between the individuals in this setting and consequently it is the only parameter having a coefficient of variation (CV).

CV = Coefficient of Variation in percent = $\frac{std}{est} \times 100$, with std the standard deviation of the lognormal distribution of the parameter and est the population estimate.

CI = Confidence Interval on the population estimate inferred from the standard errors on the fit.

Supplementary Figures

Supplementary Figure 1. In vitro fit and direct statistical analysis of the xenograft breast data (LM2-4^{luc+})

Supplementary Figure 2. Population fit of the tumor growth data that were measured by BL, under the Gomp-Exp model and initial volume V_0 fixed by the conversion rule inferred from the correlation between volume and BL ($V_0 = 10$ p/s)

Supplementary Figure 3. Population fits of the breast xenograft data under different growth theories

Supplementary Figure 4. Population fits of the kidney isograft data under different growth theories

Supplementary Figure 5. Second kidney data set used for fitting the data (resection time = 23 days)

Supplementary Figure 6. Individual fits of primary tumor and metastatic burden kinetics. Breast animal model

Supplementary Figure 7. Individual fits of primary tumor and metastatic burden kinetics. Kidney animal model

Supplementary Figure 8. Link between experimental and model survival

Supplementary Figure 9: Surgery benefit on survival and metastatic burden reduction as a function of resection size, for varying values of metastatic potential (parameter μ)

Supplementary Figure 10. Population fits of the ortho-surgical metastasis animal models for a dissemination coefficient $\mathrm{d}(\mathbf{V_p}) = \mu \mathbf{V_p^\gamma}$ and various values of γ

Supplementary Figure 11. Population fits of the ortho-surgical metastasis animal models for various values of the signal-to-cell ratio V_0

Supplementary Movie 1: Simulation of the cancer history from the first cancer cell for a virtual patient with median μ

Supplementary Movie 2: Simulation of the cancer history from the first cancer cell for a virtual patient with large μ, at the 90th percentile.

Supplementary Figure 1. In vitro fit and direct statistical analysis of the xenograft breast data (LM2-4^{luc+})

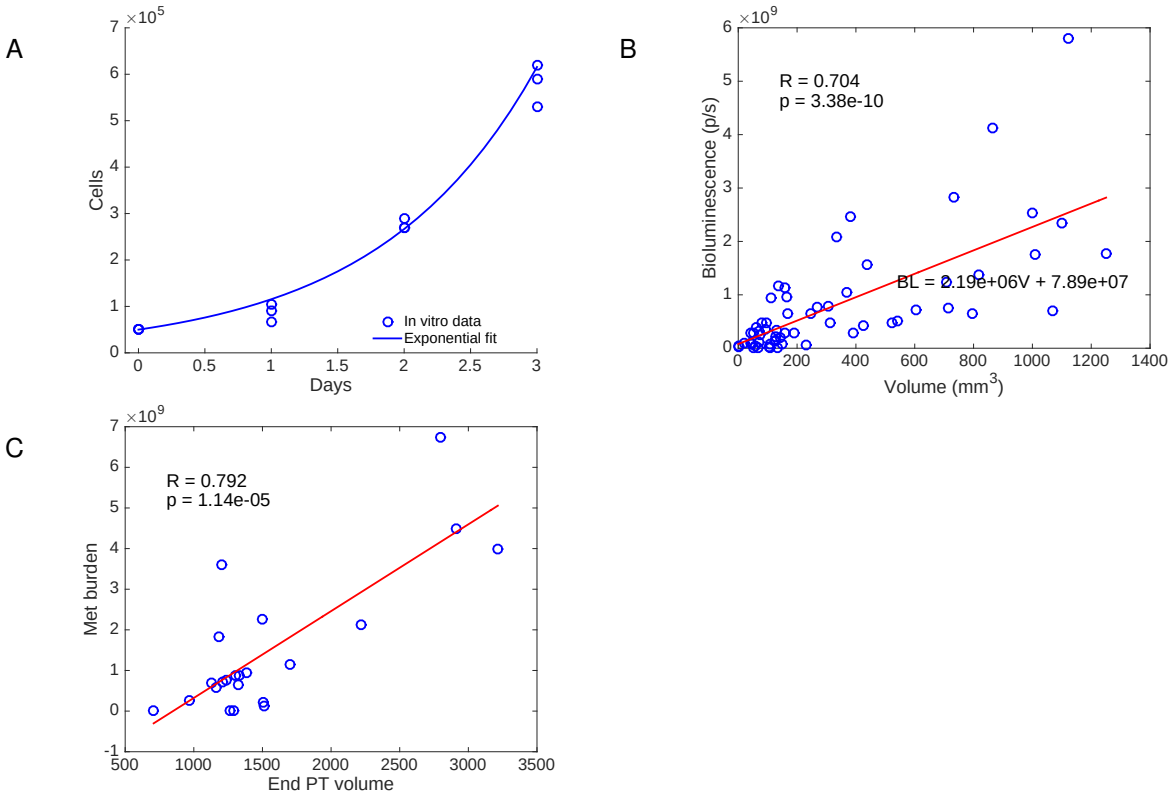

A. *In vitro* proliferation kinetics and exponential fit of the LM2-4^{luc+} cell line. Three replicates
B. Correlation between bioluminescence emission and caliper-measured volume of the primary tumor
C. Correlation between PT volume at resection and final metastatic burden
PT = Primary Tumor

Supplementary Figure 2. Population fit of the tumor growth data that were measured by BL, under the Gomp-Exp model and initial volume V_0 fixed by the conversion rule inferred from the correlation between volume and BL ($V_0 = 10$ p/s)

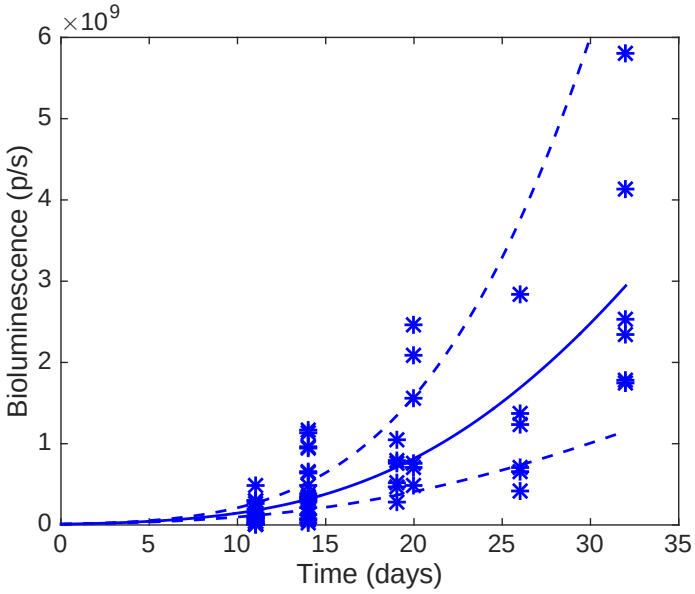

Fit was performed using nonlinear mixed effects modeling (function *nlmefitsa* of Matlab). Plain line is the median output from the model under the inferred population distribution and dashed lines are 10% and 90 % percentiles. The good quality of the fit gives an *a posteriori* rationale for the relevance of our value of V_0.

Supplementary Figure 3. Population fits of the breast xenograft data under different growth theories

A

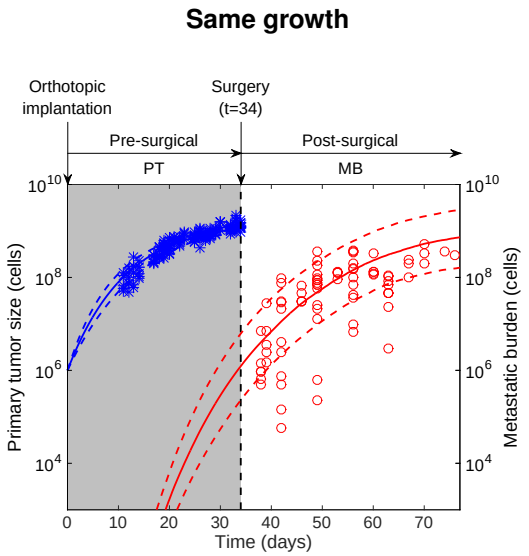

B

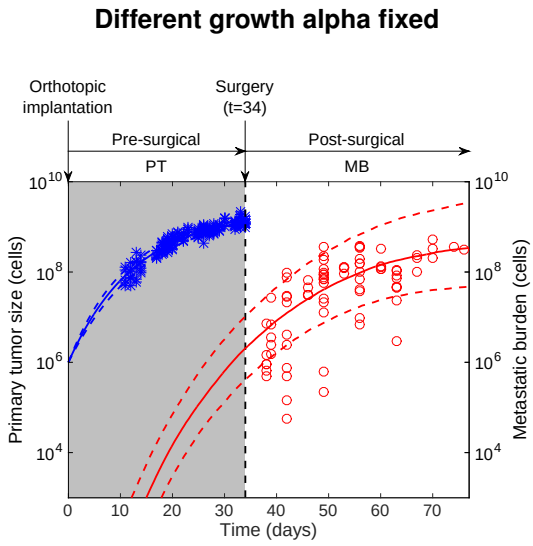

C

Model	Par.	Unit	Median value (CV)	NSE (%)
Diff growth alpha fixed	α_P	day^{-1}	0.605 (9.83)	3.57
	β_P	day^{-1}	0.0786 (12.2)	4.86
	μ	$cell^{-1} \cdot day^{-1}$	3.01e-09 (820)	72.1
	β	day^{-1}	0.0816 (15.7)	5.06
Same growth	α	day^{-1}	0.664 (16.3)	4.76
	β	day^{-1}	0.0893 (21.3)	6.21
	μ	$cell^{-1} \cdot day^{-1}$	4.43e-11 (176)	26.5

Fits of the breast xenograft data under two models.
A: Same growth = same Gompertz growth parameters (α and β) for primary and secondary tumors.
B: Different growth alpha fixed = for each animal, same value of parameter α was imposed while value of β was allowed to vary between the PT and the secondary tumors.
C: Parameters estimates under the two different models.
With similar visual accuracy of the population fits (also observable in individual fits of particular mice, data not shown), the second model generated substantially higher uncertainty on the parameter estimation, especially parameter μ, with respective normalized standard errors (NSE) of 26.5% for the “same growth” model and 72.1% for the “different growth with alpha fixed” model. Additionally, probably due to sharper estimation of the parameters, predictive performances were improved with the “same growth” model (results not shown).

Supplementary Figure 4. Population fits of the kidney isograft data under different growth theories

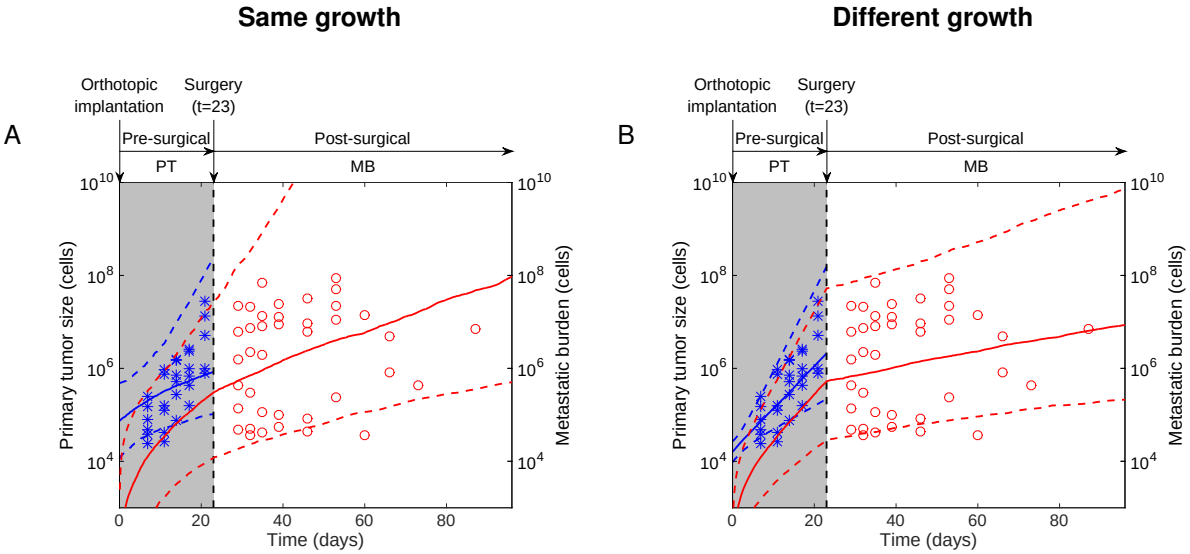

C

Model	Par.	Unit	Median value (CV)	NSE (%)
Diff growth exp	V_i	p/s	1.63e+05 (45.5)	29.9
	α_P	day^{-1}	0.21 (60.3)	17.2
	μ	$cell^{-1} \cdot day^{-1}$	0.00415 (397)	48.4
	α	day^{-1}	0.0307 (201)	48.9
Same growth exp	V_i	p/s	8.05e+05 (779)	53.7
	α	day^{-1}	0.0831 (325)	40.4
	μ	$cell^{-1} \cdot day^{-1}$	0.000892 (2.88e+03)	77.4

Fits of one of the datasets for the isograft kidney model (surgery at day 23) under two models for the growth of secondary tumors in relationship to the PT. At the structural level, both growths were considered exponential.
A: Same growth rate between primary and secondary tumors.
B: Different growth rate between primary and secondary tumors.
C: Parameters estimates under the two different models.
We chose the second model to be best adapted because: 1) the population fit was more accurate, especially for description of the inter-animal variability, 2) adding a parameter did not result in deterioration of the normalized standard errors (NSE) of the parameters estimates and 3) the low descriptive power of the “same growth” model was confirmed by a large inaccuracy in individual fits (results not shown)

Supplementary Figure 5. Second kidney data set used for fitting the data (resection time = 23 days)

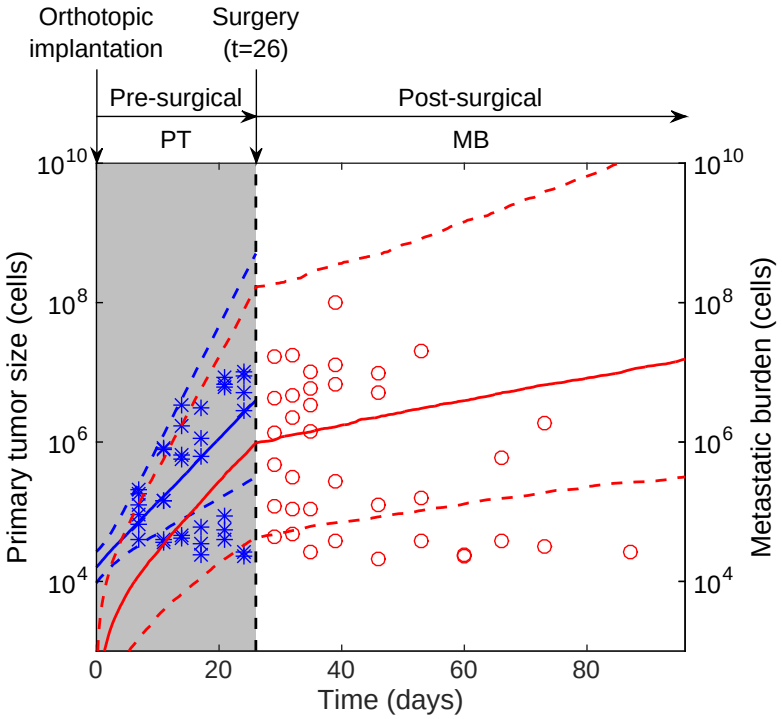

Supplementary Figure 6. Individual fits of primary tumor and metastatic burden kinetics. Breast animal model

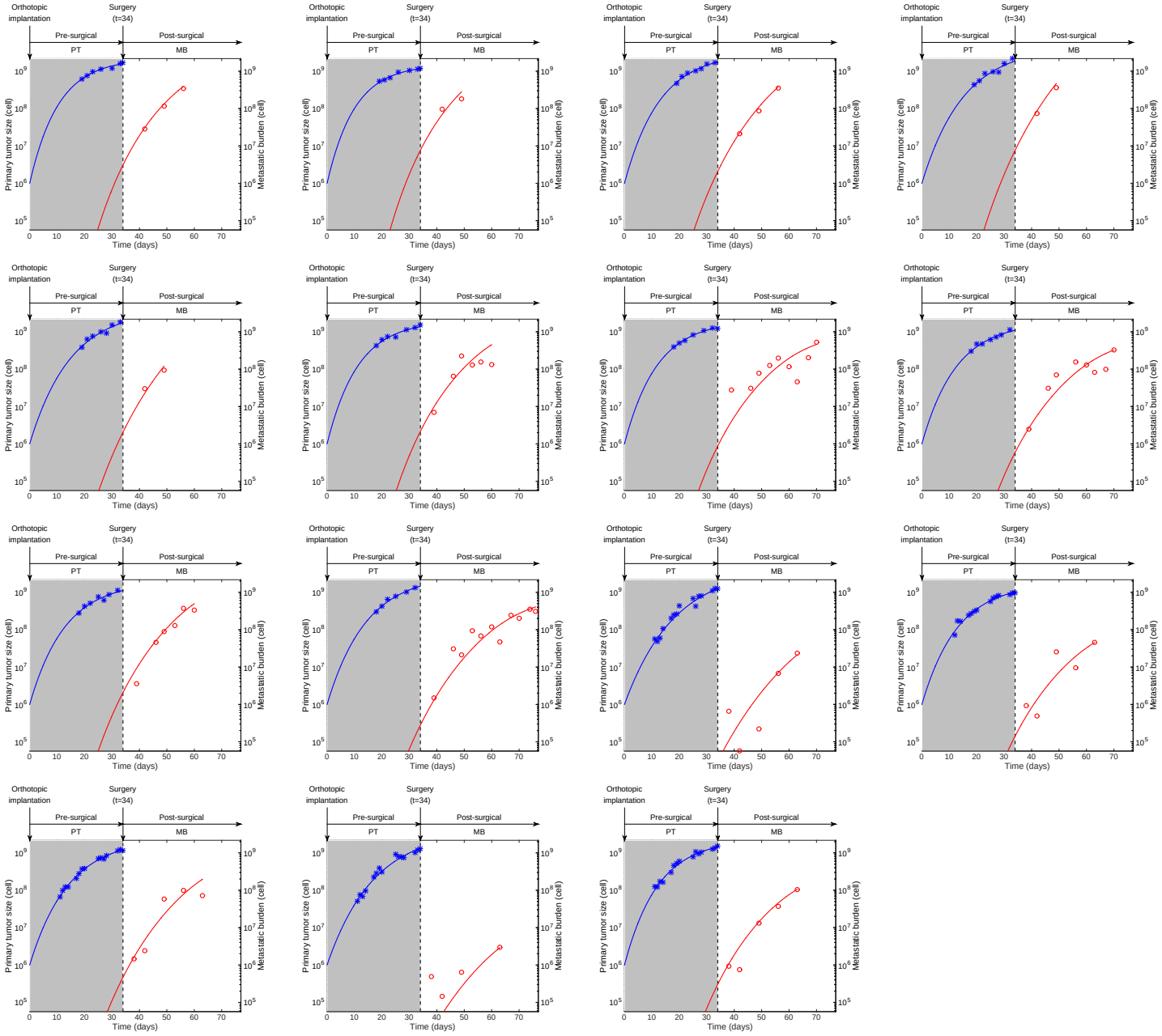

Equivalent of Figure 3 with all the animals. Each animal was fitted separately.

Supplementary Figure 7. Individual fits of primary tumor and metastatic burden kinetics. Kidney animal model

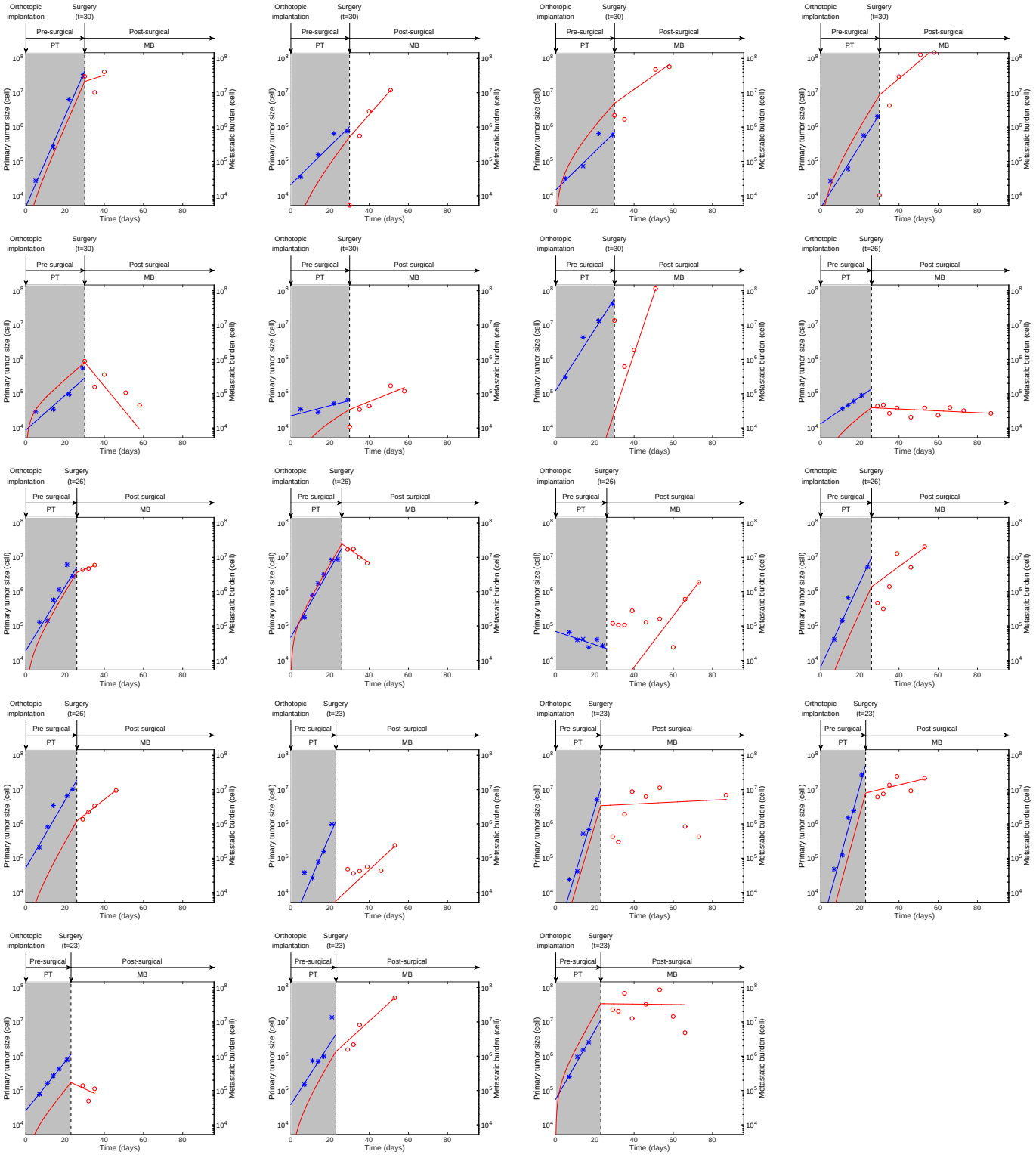

Equivalent of Figure 3 with all the animals. Each animal was fitted separately.

Supplementary Figure 8. Link between experimental and model survival

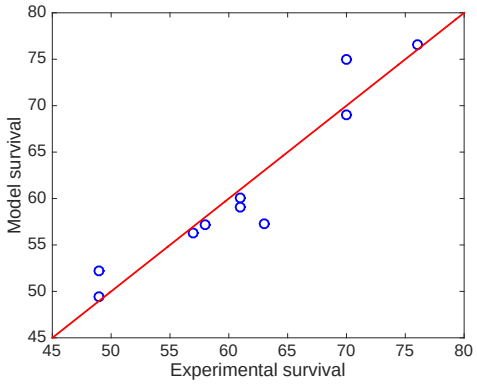

Predicted versus experimental survival. The model survival was defined as the time to reach a given lethal burden of $1 \cdot 10^{12}$ p/s, i.e. $\inf\left\{t > 0; M(t) > 1 \cdot 10^{12}\right\}$

Supplementary Figure 9: Surgery benefit on survival and metastatic burden reduction as a function of resection size, for varying values of metastatic potential (parameter μ)

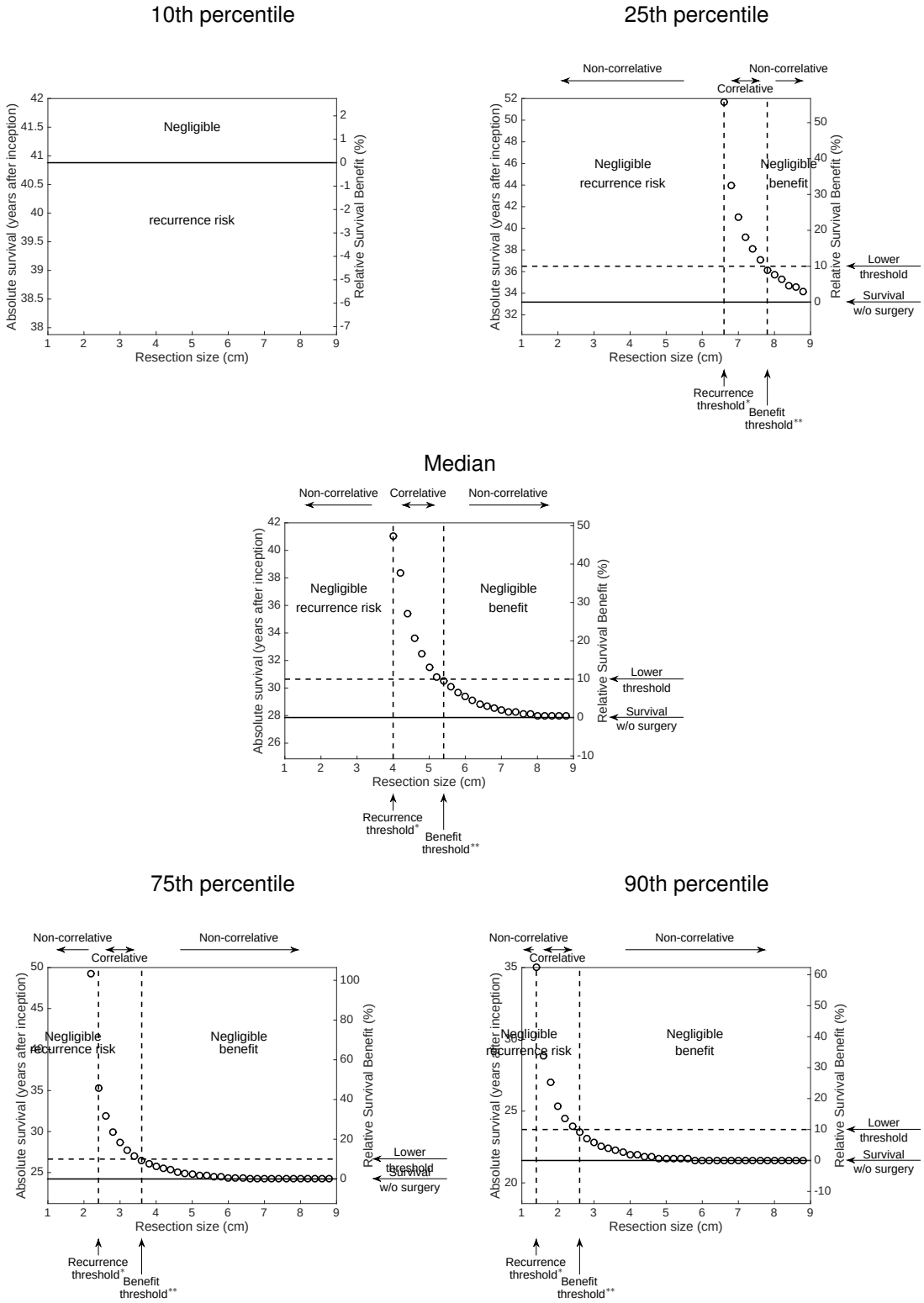

Supplementary Figure 10. Population fits of the ortho-surgical metastasis animal models for a dissemination coefficient $\mathrm{d}(\mathrm{V_p}) = \mu \mathrm{V_p^{\gamma}}$ and various values of γ

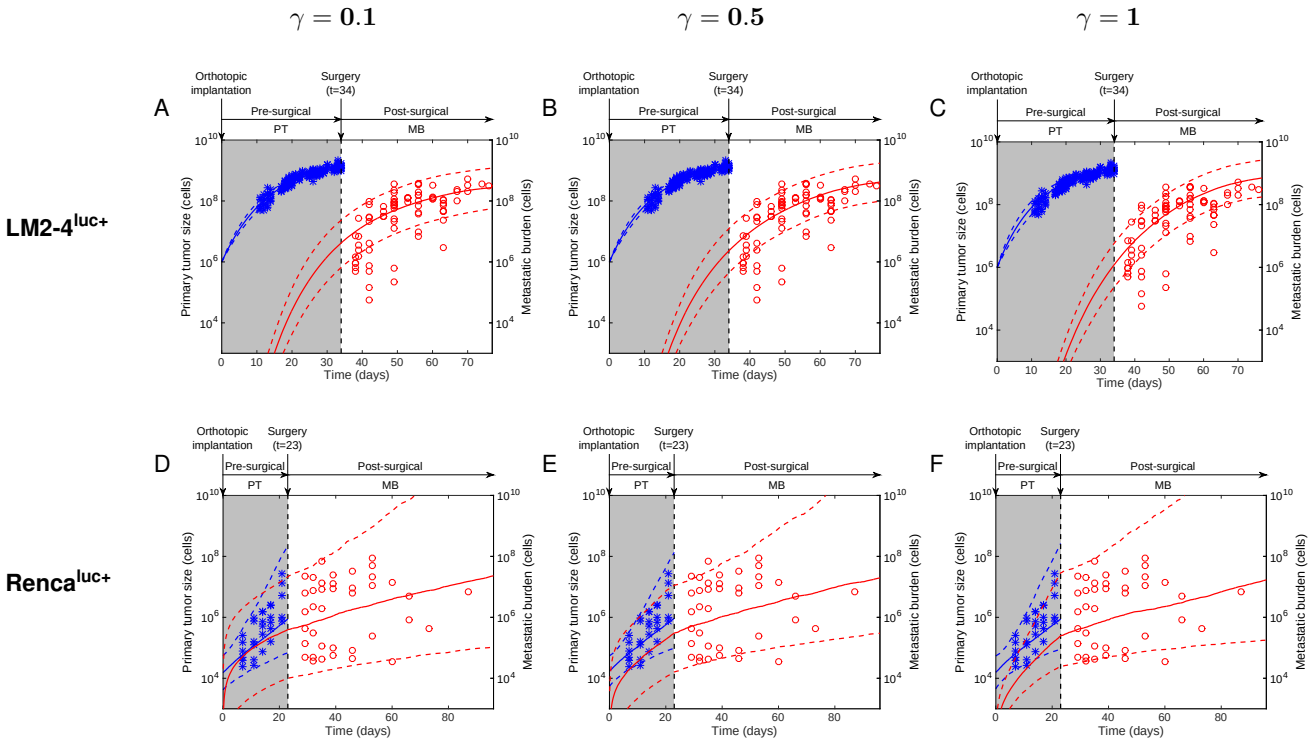

A - C: Xenograft breast model (LM2-4^{luc+})

D - E: Isograft kidney model (Renca^{luc+}). Only group with surgery at t = 23 days is shown.

Other intermediate values of γ between 0 and 1 produced similar, visually equivalent fits.

Supplementary Figure 11. Population fits of the ortho-surgical metastasis animal models for various values of the signal-to-cell ratio V_0

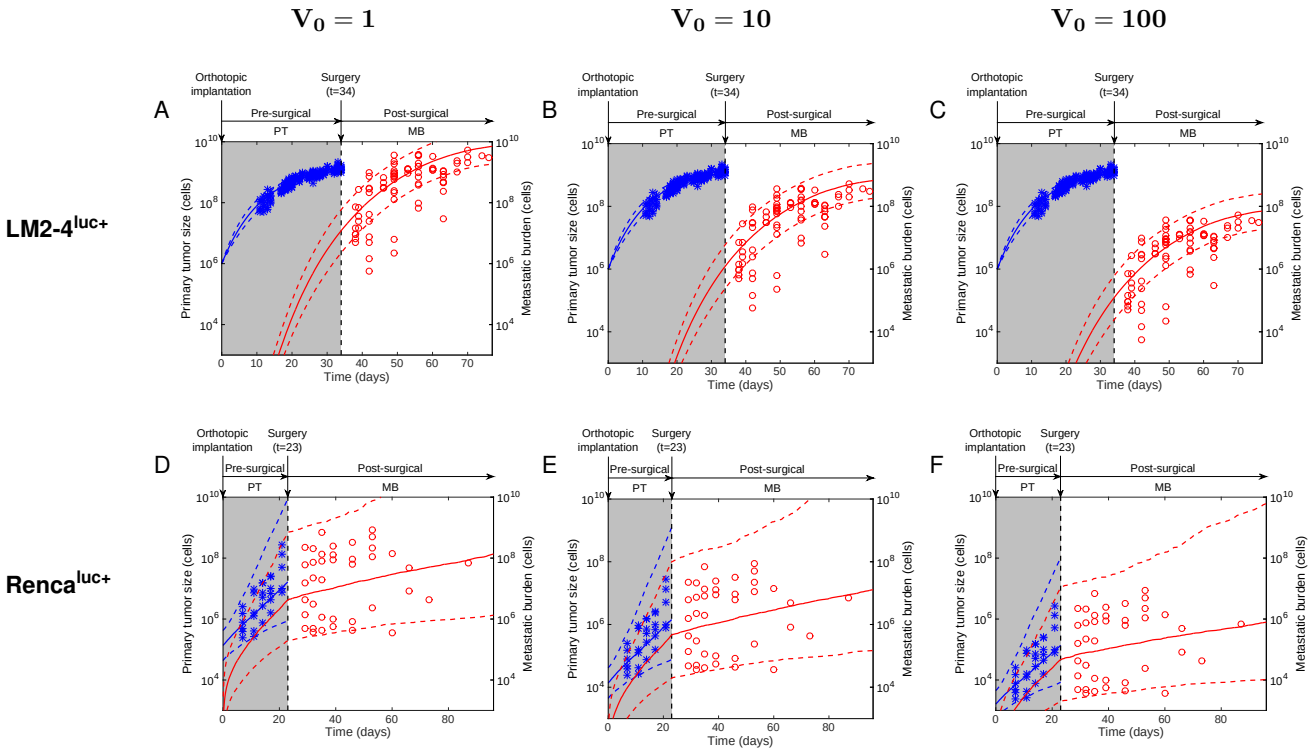

G

V_0 (p/s)	1.0	10.0	100.0
LM2-4^{luc+}	4.43×10^{-10}	4.16×10^{-11}	4.50×10^{-12}
Renca^{luc+}	0.0298	0.0348	0.0375

The relationship between BL and volume was far from perfectly linear in supplementary Figure 1B. This suggests that, for detectable volumes, the number of living tumor cells might not be proportional to the tumor volume, consistently with general laws of tumor growth (37). Hence, considering the relatively poor reliability of the extrapolated value of V_0, simulations were performed to test the robustness of the results with respect to the value of V_0, by varying V_0 over two orders of magnitude. Similar fits were obtained for the metastatic burden (MB) (supplementary Figure 10), showing that, for our concern here (the MB), different values of V_0 were virtually equivalent.

A - C: Xenograft breast model (LM2-4^{luc+})

D - E: Isograft kidney model (Renca^{luc+}). Only group with surgery at t = 23 days is shown.

Goodness-of-fit performances were the same for each value of V_0. The data is shifted along the y-axis because the conversion rule was used to convert the bioluminescence data into cell numbers. For the breast data, primary tumor volumes were measured in mm^3 using calipers and then converted into cell numbers using the conversion rule 1 mm$^3 \simeq 10^6$ cells. Hence, the conversion did not depend on V_0 and the data was not shifted when changing V_0.

G: Population estimate of μ (in cell$^{-1}\cdot$ day^{-1}) for the different values of V_0.

Supplementary Movie 1: Simulation of the cancer history from the first cancer cell for a virtual patient with median μ

Primary tumor (PT) was assumed to be detected when reaching the size of 4.32 cm in diameter. Post-diagnosis PT growth and development of metastases in the case of no surgical intervention are indicated as dashed line in the left plot and white bars in the histogram on the right, respectively.

Supplementary Movie 2: Simulation of the cancer history from the first cancer cell for a virtual patient with large μ, at the 90th percentile.

Primary tumor (PT) was assumed to be detected when reaching the size of 4.32 cm in diameter. Post-diagnosis PT growth and development of metastases in the case of no surgical intervention are indicated as dashed line in the left plot and white bars in the histogram on the right, respectively.

Supplementary text

Using the model from [Hartung et al., 2014] on the LM2-4^{luc+} data

In [Hartung et al., 2014], Hartung, Mollard et al. had developed a similar modeling analysis on data from breast cancer xenografts, however with no consideration of primary tumor surgery and in severely immune-incompetent mice. Thus, it could have been interesting to see whether the modeling analysis brings any insights on the differences between the cases with and without surgery. Unfortunately, quantitative comparison was hampered by the following points: different number of cells injected, different mice strain (severe combined immuno-deficient in our case versus Nod-scid gamma in their case), different bioluminescence quantification method (2D versus 3D) that resulted in a different cell-to-signal ratio and integration of peritoneal metastases for them versus only pulmonary metastases for us. Keeping all these flaws in mind, we nevertheless applied their model to our ortho-surgical data set of breast xenografts. This consisted in the use of a dissemination coefficient with the form $d(V_p) = \mu V_p^{2/3}$, different growth rates for the primary tumor and the metastases, and a different parameterization of the Gompertz growth rate, written as: $g(V) = aV \ln\left(\frac{b}{V}\right)$. We obtained a significantly larger value of a in our data of 4.91×10^{-2} day^{-1} $\pm\, 2.02 \times 10^{-3}$ versus 7.9×10^{-3} day^{-1} $\pm\, 2.5 \times 10^{-3}$ in [Hartung et al., 2014] (population estimate $\pm$ standard error). This could suggest post-surgery acceleration of metastases. On the other hand, the value of μ was also found significantly different, with several order of magnitudes of difference. We computed $\mu = 7.24 \times 10^{-3} \pm 8.5 \times 10^{-3}$ cell$^{-2/3}\cdot$ day^{-1} versus $\mu = 6.31 \times 10^{-1} \pm 4.42 \times 10^{-1}$ cell$^{-2/3}\cdot$ day^{-1} in [Hartung et al., 2014]. Indeed, it was already visible in the data without performing any quantitative analysis that they obtained a larger metastatic burden for smaller primary tumor sizes.

Supplementary methods

Preclinical methodology

Ortho-surgical models of metastasis

For ortho-surgical metastasis models, we followed detailed experimental criteria to control for variable disease progression and model standardization as previously described [Ebos et al., 2014]. For example, in breast (LM2-4^{LUC+}) and kidney (RENCA^{LUC+}) models, tumor invasion noted during surgery such as growth into peritoneal space (breast) or presentation of a non-encapsulated kidney tumor led to mouse exclusion from study. Additionally, if no tumor was present at any time before and after surgery (determined by bioluminescence or visible macroscopically), mice were excluded from study so as not to give potential false positive or negative bias to results (see [Ebos et al., 2014]). Note: all animals used in this study represent vehicle-treated controls from published [Ebos et al., 2014] and unpublished studies involving sunitinib malate. Therefore all animals in this study were treated with 10ml/kg vehicle for 7-14 days prior to tumor resection. Vehicle contained carboxymethylcellulose sodium (USP, 0.5% w/v), NaCl (USP, 1.8% w/v), Tween-80 (NF, 0.4% w/v), benzyl alcohol (NF, 0.9% w/v), and reverse osmosis deionized water (added to final volume) and adjusted to pH 6 (see [Ebos et al., 2008]). Importantly, no difference in metastatic disease progression patterns or survival has been observed between vehicle and untreated animals ([Ebos et al., 2014] and data not shown).

Bioluminescent imaging

Quantification of local and disseminated tumor burden by bioluminescent imaging has been previously described in detail (see [Ebos et al., 2014] and [Ebos et al., 2008]). Briefly, mice were injected intraperitoneally with substrate D-luciferin at 150 mg/kg in Dulbecco's

Phosphate Buffered Saline (Corning, Cat. #MT21-031-CV) and, after a 10 minute interval, anesthetized (4% isoflurane in oxygen for induction, 2% for maintenance) and placed onto the warmed stage inside the light-tight camera box (IVIS™ ; Xenogen, Alemeda, CA) as previously described ([Ebos et al., 2009] and [Ebos et al., 2014]). Light emitted from bioluminescent cells after 1 minute was detected by the IVIS® camera system with images quantified for tumor burden using a log-scale color range set at 5×10^4 to 1×10^7 and measurement of total photon counts per second (p/s) using Living Image software (Xenogen)

Mathematical methodology: Stochastic dynamics of metastasis formation

The formalism we employed to fit the model to the data was deterministic, because fast simulations were required for the large number of computations of the model needed for fitting the data. However, when considering simulation of individual dynamics (Figure 4), stochastic dynamics were simulated. The stochasticity here refers to intra-individual randomness in the metastatic dissemination. The stochastic version of the model was the following. The formation of new metastatic foci was assumed to be a sequence of random events exponentially distributed with rate $d(V_p(t))$. The number of metastases followed then a Poisson process $\mathcal{N}(t)$ with intensity $d(V_p(t))$. The appearance time of the i-th metastasis was defined by

$$T_i = \inf \{t \geq 0;\ N(t) \geq i\}$$

Adapting the methodology of [Iwata et al., 2000] to the case of randomly distributed dissemination times and denoting $\tilde{\rho}$ the resulting random size distribution of metastases, $\tilde{\rho}$ was a sum of Dirac masses solving the following problem

$$\begin{cases} \partial_t \tilde{\rho}(t,v) + \partial_v(\tilde{\rho}(t,v)g(v)) = 0 & t \in]0,+\infty[,\ v \in]V_0,+\infty[\\ g(V_0)\tilde{\rho}(t,V_0) = \sum_{i=1}^{+\infty} \delta\left(t = T_i\right) & t \in]0,+\infty[\\ \tilde{\rho}(0,v) = 0 & v \in]V_0,+\infty[\end{cases} \tag{1}$$

Equivalently, denoting by V_i the volume of the i-th metastasis, we have

$$\begin{cases} \frac{dV_i}{dt} = g(V_i(t)) \\ V_i(T_i) = V_0, \quad V_i(t) = 0, \text{ for } t \leq T_i \end{cases}$$

From these considerations the stochastic total metastatic burden at time t, denoted by $\mathcal{M}(t)$ was defined by

the following expression

$$\mathcal{M}(t) = \int_{V_0}^{+\infty} v\tilde{\rho}(t,v)dv = \sum_{i=1}^{+\infty} V_i(t)$$

The two approaches (deterministic and stochastic) are in fact closely and consistently linked. It can be shown [Hartung and Christophe, 2014] that the quantities $M(t)$ and $N(t)$ defined in the body text (section "quick guide to equations and assumptions") are the respective expectations of $\mathcal{M}(t)$ and $\mathcal{N}(t)$.

References

[Ebos et al., 2008] Ebos, J. M. L., Lee, C. R., Bogdanovic, E., Alami, J., Van Slyke, P., Francia, G., Xu, P., Mutsaers, A. J., Dumont, D. J., and Kerbel, R. S. (2008). Vascular endothelial growth factor-mediated decrease in plasma soluble vascular endothelial growth factor receptor-2 levels as a surrogate biomarker for tumor growth. *Cancer Res*, 68(2):521–529.

[Ebos et al., 2009] Ebos, J. M. L., Lee, C. R., Cruz-Munoz, W., Bjarnason, G. A., Christensen, J. G., and Kerbel, R. S. (2009). Accelerated metastasis after short-term treatment with a potent inhibitor of tumor angiogenesis. *Cancer Cell*, 15(3):232–239.

[Ebos et al., 2014] Ebos, J. M. L., Mastri, M., Lee, C. R., Tracz, A., Hudson, J. M., Attwood, K., Cruz-Munoz, W. R., Jedeszko, C., Burns, P., and Kerbel, R. S. (2014). Neoadjuvant antiangiogenic therapy reveals contrasts in primary and metastatic tumor efficacy. *EMBO Mol Med*, 6(12):1561–1576.

[Hartung and Christophe, 2014] Hartung, N. and Christophe, G. (2014). A stochastic framework for secondary metastatic emission.

[Hartung et al., 2014] Hartung, N., Mollard, S., Barbolosi, D., Benabdallah, A., Chapuisat, G., Henry, G., Giacometti, S., Iliadis, A., Ciccolini, J., Faivre, C., and Hubert, F. (2014). Mathematical modeling of tumor growth and metastatic spreading: validation in tumor-bearing mice. *Cancer Res*, 74(22):6397–6407.

[Iwata et al., 2000] Iwata, K., Kawasaki, K., and Shigesada, N. (2000). A Dynamical Model for the Growth and Size Distribution of Multiple Metastatic Tumors. *J Theor Biol*, 203(2):177–186.